Clim. Past, 11, 115–133, 2015
www.clim-past.net/11/115/2015/
doi:10.5194/cp-11-115-2015

Climate of the Past
Open Access

Simulating ice core ^{10}Be on the glacial–interglacial timescale

C. Elsässer[1], D. Wagenbach[1,†], I. Levin[1], A. Stanzick[1], M. Christl[2], A. Wallner[3], S. Kipfstuhl[4], I. K. Seierstad[5], H. Wershofen[6], and J. Dibb[7]

[1]Institut für Umweltphysik, University of Heidelberg, Im Neuenheimer Feld 229, 69120 Heidelberg, Germany
[2]Laboratory for Ion Beam Physics, ETH Zurich, 8093 Zurich, Switzerland
[3]Vienna Environmental Research Accelerator, University of Vienna, 1090 Vienna, Austria
[4]Alfred Wegener Institute for Polar and Marine Research, 27570 Bremerhaven, Germany
[5]Centre for Ice and Climate, University of Copenhagen, 2100-Copenhagen, Denmark
[6]Physikalisch-Technische Bundesanstalt, 38116 Braunschweig, Germany
[7]Institute for the Study of Earth, Oceans, and Space, University of New Hampshire, Durham, NH 03824, USA
[†]deceased, 4 December 2014

Correspondence to: C. Elsässer (christoph.elsaesser@iup.uni-heidelberg.de)

Received: 29 January 2014 – Published in Clim. Past Discuss.: 26 February 2014
Revised: 25 November 2014 – Accepted: 7 December 2014 – Published: 3 February 2015

Abstract. ^{10}Be ice core measurements are an important tool for paleoclimate research, e.g., allowing for the reconstruction of past solar activity or changes in the geomagnetic dipole field. However, especially on multi-millennial timescales, the share of production and climate-induced variations of respective ^{10}Be ice core records is still up for debate. Here we present the first quantitative climatological model of the ^{10}Be ice concentration up to the glacial–interglacial timescale. The model approach is composed of (i) a coarse resolution global atmospheric transport model and (ii) a local ^{10}Be air–firn transfer model. Extensive global-scale observational data of short-lived radionuclides as well as new polar ^{10}Be snow-pit measurements are used for model calibration and validation. Being specifically configured for ^{10}Be in polar ice, this tool thus allows for a straightforward investigation of production- and non-production-related modulation of this nuclide. We find that the polar ^{10}Be ice concentration does not immediately record the globally mixed cosmogenic production signal. Using geomagnetic modulation and revised Greenland snow accumulation rate changes as model input, we simulate the observed Greenland Summit (GRIP and GISP2) ^{10}Be ice core records over the last 75 kyr (on the GICC05modelext timescale). We show that our basic model is capable of reproducing the largest portion of the observed ^{10}Be changes. However, model–measurement differences exhibit multi-millennial trends (differences up to 87 % in case of normalized to the Holocene records) which call for closer investigation. Focusing on the (12–37) b2k (before the year AD 2000) period, mean model–measurement differences of 30 % cannot be attributed to production changes. However, unconsidered climate-induced changes could likely explain the model–measurement mismatch. In fact, the ^{10}Be ice concentration is very sensitive to snow accumulation changes. Here the reconstructed Greenland Summit (GRIP) snow accumulation rate record would require revision of +28 % to solely account for the (12–37) b2k model–measurement differences.

1 Introduction

Cosmogenic ^{10}Be has become a common quantity measured in polar ice cores since trailblazing investigations were performed decades ago (Raisbeck et al., 1981; Yiou et al., 1985; Beer et al., 1985). Today, more than 20 different ice cores from Greenland and Antarctica provide ^{10}Be records on various timescales up to more than 100 kyr. Being produced by interactions of cosmic rays with atmospheric nitrogen and oxygen, ^{10}Be quickly gets attached to sub-micron aerosol particles and is removed from the atmosphere by wet and dry deposition processes, including deposition onto polar glaciers. Research attempts therefore use ice core ^{10}Be as proxy for past changes of its cosmogenic production rate and

the related solar and geomagnetic activity (Beer et al., 1988; Raisbeck et al., 1990; Bard et al., 1997; Muscheler et al., 2005; Vonmoos et al., 2006; Muscheler et al., 2007; Steinhilber et al., 2012). However, due to aerosol-related transport and deposition processes of ^{10}Be, respective ice core records also hold information on past climate variability making this cosmogenic radionuclide also a valuable tool for estimating past snow accumulation rate changes (Mazaud et al., 1994; Steig, 1996; Wagner et al., 2001b). The question of whether to use ^{10}Be ice concentration records as proxy for production or climate variability depends on the timescale under investigation as well as on the local climate conditions of the concerned drilling site. In either case, the detailed understanding of production- and non-production-related influences on the polar ^{10}Be ice concentration is an important requirement for the interpretation of the ^{10}Be ice core records.

In recent years, several studies improved the knowledge on processes which influence atmospheric ^{10}Be in polar regions. Atmospheric production rates have been calculated within elaborative Monte Carlo simulations of cosmic ray particle cascades (Masarik and Beer, 2009; Kovaltsov and Usoskin, 2010). Long-term records of radionuclide air concentrations (e.g., Dibb, 2007; Aldahan et al., 2008; Elsässer et al., 2011) as well as high-resolution measurements of ^{10}Be in snow and firn (Pedro et al., 2006, 2011) have been evaluated for the understanding of radionuclide transport processes while global circulation modeling studies investigated the climate influence on the ^{10}Be deposition (Field et al., 2006; Heikkilä et al., 2008a, 2009, 2013). However, despite these efforts, several findings remain inconsistent, making the interpretation of ^{10}Be ice core records a matter of ongoing debate. Further research needs concern transport and deposition processes, linking the ^{10}Be ice concentration with the cosmogenic production in the atmosphere. Measurements of ^{10}Be (and short-lived ^{7}Be) in polar air show that its boundary layer concentration is very sensitive to seasonal changes in atmospheric circulation processes such as the stratosphere–troposphere exchange or vertical tropospheric mixing (Elsässer et al., 2011). So far it is up for debate as to how these processes are subject to longer-term climate changes and modulate the ^{10}Be ice concentration. In addition to direct effects of atmospheric transport on ^{10}Be, atmospheric mixing has a major influence on the production signal recorded in ice core ^{10}Be: while geomagnetic changes primarily affect atmospheric ^{10}Be production at lower latitudes, solar-activity-based production variations are more decisive in polar areas. Detailed knowledge of the ^{10}Be atmospheric footprint is thus a crucial requirement for interpreting observed ^{10}Be time series. Moreover, in addition to atmospheric transport, aerosol deposition is a crucial process influencing the ^{10}Be ice concentration. While during the Holocene period ^{10}Be variations are dominated by production changes related to solar and geomagnetic activity (e.g., Steinhilber et al., 2012), ^{10}Be ice concentration is certainly subject to climate modulation on longer timescales (e.g., Finkel and Nishiizumi, 1997). Here, strong changes in the snow accumulation rate (up to a factor of 2–10 in the case of the transition from glacial to Holocene conditions) certainly alter the ^{10}Be ice concentration. However, the modulation of the ^{10}Be ice core records by snow accumulation changes essentially depends on the site-specific ratio of dry to wet deposition which is still a matter of debate for every single ice core record.

Regarding these uncertainties in the interpretation of ^{10}Be ice concentration, there is a strong need for modeling attempts to simulate ^{10}Be ice core records; however, adequate models do not yet exist. On the one hand, conceptual models, which are generally used for the interpretation of ^{10}Be ice core measurements, oversimplify the processes influencing ice core ^{10}Be. On the other hand, complex global circulation models (GCM), which allow for the investigation of detailed climate-driven ^{10}Be transport and deposition processes, are still restricted to the decennial timescale (see, e.g., Heikkilä et al., 2013 for the latest results on this issue). Indeed, there is a strong need for multi-millennia simulations since both production and climate modulation of ^{10}Be also occur on long timescales. Future work will likely expand complex models to simulate longer, multi-millennial timescales. However, custom-made models of lower complexity are needed now to improve our interpretation of ice core ^{10}Be.

In this paper we present such a model which allows for the first simulations of the ^{10}Be ice concentration on the glacial–interglacial timescale. To do so, we make use of our long-standing investigations of aerosol-bound radionuclides in polar regions to balance simplicity and validity of the model approach. The basic idea of the model setup is based on the finding that spatial variability of the polar ^{10}Be ice concentration mainly relies on air–firn transfer processes (e.g., Stanzick, 2001). Here, air–firn transfer comprises all processes incorporating particles into the near-surface firn layer (e.g., wet and dry deposition, air pumping, snow drift scavenging and sedimentation). Indeed, monitoring of radionuclide air concentration in polar areas reveals that climatological features (e.g., the decadal scale, mean air concentration or the average seasonal cycle) of atmospheric ^{10}Be have large spatial validity (e.g., Dibb et al., 1994; Elsässer et al., 2011). Our model approach is thus split into (i) a coarse resolution model of the global atmosphere which allows for multi-millennial simulations of the polar ^{10}Be boundary layer air concentration, and (ii) a local air–firn transfer model which simulates the hand over from ^{10}Be air concentration to ice concentration for a specific drilling site. For simulating the global atmosphere, we use the well-established multi-box Global RadioCarbon Exploration model (GRACE) (Levin et al., 2010b) together with extensive long-term, global-scale observations of short-lived, aerosol-borne radionuclides. The air–firn transfer model is essentially predicated on new ^{10}Be measurements within several polar traverses (Stanzick, 2001; Elsässer, 2013). In the following, we describe the model setup in detail (Sect. 2 and Supplement) and subsequently present model results and implications for the extensively

used Greenland Summit (GRIP and GISP2) ice core records (Finkel and Nishiizumi, 1997; Yiou et al., 1997; Wagner et al., 2001a; Muscheler et al., 2004) for the last 75 kyr (Sect. 3).

2 Model setup

2.1 Global atmospheric transport of aerosol-borne radionuclides

Intending to simulate climatological (i.e., mean state of climate) features of the polar boundary layer ^{10}Be air concentration, we aim for an easy-to-use model setup which meets two different demands: (i) the model should be simple enough to allow for multiple long-term (glacial–interglacial) simulations under different scenarios on atmospheric transport; (ii) it should be of adequate complexity to quantitatively reproduce the main climatological features of atmospheric ^{10}Be like its prominent seasonal cycle. Tackling this task, the main idea of our approach is to combine a well-established multi-box model of the global atmosphere with the extensive history of radionuclide observations within atmospheric nuclear bomb test monitoring. Initiated from atmospheric nuclear weapon tests in the early 1950s, wide monitoring programs provide (multi-decadal) observations of short-lived bomb fission and natural radionuclides on the global scale (e.g., HASL, 1977; Leifer and Juzdan, 1986; Larsen et al., 1995). Within the present study, we use ^{137}Cs, ^{90}Sr, ^{210}Pb and ^{7}Be air concentration and ^{90}Sr deposition measurements to adapt the multi-box model GRACE (Levin et al., 2010b) for the simulation of aerosol-borne radionuclides. In addition to published radionuclide measurement data, global-scale observations of atmospheric ^{7}Be from the preparatory commission for the Comprehensive nuclear-Test-Ban Treaty Organization (UN CTBTO) International Monitoring System (IMS) are for the first time presented and applied for model validation.

2.1.1 The GRACE model

The GRACE model was developed to simulate and investigate the circulation of bomb radiocarbon in the atmosphere (Hesshaimer, 1997; Naegler, 2005; Levin et al., 2010b). The model is thus specifically calibrated to account for (seasonal) stratosphere–troposphere exchange (STE), making it an ideal tool to simulate cosmogenic radionuclides in the atmosphere. In recent years, the GRACE model was proved to be well suited for global-scale investigations of greenhouse gases and their isotopic signature (Naegler and Levin, 2006; Levin et al., 2010a, b; C. Veidt, unpublished data), covering a period of time from the preindustrial era to date. The model setup is a two-dimensional box model of the global atmosphere. Since main atmospheric processes which influence the climatological ^{10}Be air concentration show major variations on the latitudinal scale (e.g., production, stratosphere–troposphere exchange and precipitation), the 2-D setup is a reasonable first-order approach. Model boxes represent the main features of the global atmosphere: a vertical division into planetary boundary layer (PBL), free troposphere (FT) and three stratospheric subdivisions, namely, low stratosphere (LS), middle stratosphere (MS) and high stratosphere (HS). The horizontal breakdown of the model is 30° in the free troposphere and stratospheric layers which represents the three main atmospheric circulation cells (Hadley, Ferrel and Polar cell). The resolution of the boundary layer boxes has been enlarged to 10° per box within this study. Air mass transport is calibrated using extensive global observations of bomb radiocarbon and SF_6 (see Supplement of Levin et al., 2010b). In the Southern Hemisphere extratropics, the observed seasonal cycle of the (boundary layer) ^{10}Be / ^{7}Be ratio is used to calibrate seasonal variations of the stratosphere–troposphere exchange. Three basic transport processes are involved in the model setup: diffusive air mass exchange, Brewer–Dobson circulation and tropopause height variations. Given the climatological approach, the air mass transport is not varied interannually but considers seasonal variations. A basic sketch of the model as well as further model details are shown in the Supplement (Sect. S1).

2.1.2 Modifications of the GRACE model

Implementation of the aerosol-borne radionuclides ^{10}Be, ^{7}Be, ^{137}Cs, ^{90}Sr and ^{210}Pb into GRACE required essential modifications of the model. At first, the model was upgraded with atmospheric sources of the different nuclides (see Sect. S1 for further details): in the case of cosmogenic ^{7}Be and ^{10}Be, recent studies on production rates reveal significant differences and we therefore use two different production rate calculations: Usoskin and Kovaltsov (2008) (i.e., Kovaltsov and Usoskin, 2010) and Masarik and Beer (2009). Sources of the anthropogenic bomb fission nuclides ^{137}Cs and ^{90}Sr are based on the data given in UNSCEAR (2000), while the ^{210}Pb source is calculated online from ^{222}Rn decay in the atmosphere. For the latter purpose ^{222}Rn is implemented using a global source adapted from Conen and Robertson (2002). Subsequently, the model setup was upgraded with an aerosol gravitational settling module based on aerosol physics calculations (see Sect. S1 for details). Being the only atmospheric sink for aerosol-borne radionuclides in addition to radioactive decay, the atmospheric boundary layer boxes required major modifications. We increased the horizontal resolution of the boundary layer to 10° since the global distribution of aerosol sinks mainly correlates with the global distribution of precipitation (e.g., Heikkilä and Smith, 2013). In the case of Antarctica, this boundary layer resolution broadly captures the three main climatological realms: the high Antarctic plateau (80–90° S), coastal areas (70–80° S) and the Antarctic Peninsula with the surrounding ocean (60–70° S). In contrast, the Greenland ice sheet only represents a minor part of the Arctic. We thus implemented a separate box for the Greenland ice sheet boundary layer, cou-

pled to the free polar troposphere and the surrounding Arctic basin boxes. This results in an atmospheric model setup with a total of 41 boxes. Wet and dry deposition was integrated into every boundary layer box using (i) the dry deposition velocity, (ii) precipitation rates (Global Precipitation Climatology Project, Adler et al., 2003) and (iii) the radionuclide air to rain concentration ratio (scavenging ratio). Eventually, we tuned the model to quantitatively reproduce measured ^{137}Cs and ^{90}Sr air concentrations (Feely et al., 1981, 1985, 1988; Larsen and Sanderson, 1990, 1991; Larsen et al., 1995; Kolb, 1992) and ^{90}Sr deposition flux measurements (UNSCEAR, 2000; Roos et al., 1994) by varying the scavenging ratio as well as the diffusive boundary layer–free troposphere air mass transport for every 10° box (see details on the calibration strategy in Sect. S1). Dry deposition velocity was held constant globally (except for slightly different values in the case of the ice sheet boxes, see below). Regarding the primary focus of this work being on ice core ^{10}Be, calibration of polar boxes required special consideration. Since the data basis used for global radionuclide sink calibration (^{90}Sr and ^{137}Cs measurements) lacks sufficient coverage in polar areas, we altered the calibration strategy for the Greenland and Antarctic ice sheet boxes. In brief, we use our estimation of scavenging ratios and dry deposition velocities based on ^{10}Be and ^{7}Be observations together with the air–firn transfer model (given in Sect. 2.2) and revised precipitation rates (Bales et al., 2001; Arthern et al., 2006; HASL, 1977; Larsen, 1985; Juzdan, 1988; see details in Sect. S1.6). In doing so, the remaining parameter to be specified is the diffusive air mass exchange between the ice sheet boundary layer and the free polar troposphere. So far, we use extensively measured atmospheric concentrations of ^{7}Be (Dibb, 2007; Elsässer et al., 2011) to calibrate the PBL–FT coupling of the ice sheet boxes (see Sect. S1.6 for details on the parameters). In doing so, we use the Usoskin and Kovaltsov (2008) ^{7}Be production rate calculations for model simulations. Model calibration of the ice sheet radionuclide sinks is thus not independent from ^{10}Be and ^{7}Be observations. However, the polar radionuclide sinks contribute only marginally to the global-scale sink. Therefore, the global circulation of aerosol-bound radionuclides can still be validated with ^{7}Be measurements (see Sect. 2.1.3). In a final step we used observations of atmospheric ^{210}Pb, ^{137}Cs and ^{90}Sr for additional fine-tuning of radionuclide transport and deposition processes. This fine-tuning accounts for different processes like the Arctic haze phenomenon at northern polar latitudes or ice sheet boundary layer inversion seasonality (see Sects. S1.5 and S1.6).

2.1.3 Model validation

Validation of the global atmospheric model is performed using extensive observations of short-lived atmospheric ^{7}Be on the global scale (Feely et al., 1967, 1981, 1985, 1988; Larsen and Sanderson, 1990, 1991; Larsen et al., 1995; Leifer and Juzdan, 1986; Leifer, 1992; Kolb, 1992, Durana et al., 1996; Megumi et al., 2000; Ioannidou et al., 2005; Wershofen and Arnold, 2005; Kulan et al., 2006; Kulan, 2007; Chae et al., 2011; Elsässer et al., 2011; Leppänen et al., 2012; Doering, 2007, and references therein). To do so we compare measurements at single sites with the model results for respective latitudes (see Fig. 1). In the case of the US Environmental Surface Air Sampling Program data (EML SASP – Feely et al., 1981, 1985, 1988; Larsen and Sanderson, 1990, 1991; Larsen et al., 1995), measurements used for model calibration (^{137}Cs and ^{90}Sr) and model validation (^{7}Be) originate at the same sampling sites. We therefore additionally compare our model results to observations of ^{7}Be within the CTBTO IMS. This global monitoring program provides so far unpublished measurements from 62 globally distributed sites (different from the EML program sites) covering up to 10 years. The model results for model validation cover the observational period (AD 1950–2000). The production variability of ^{7}Be is driven by reconstructions of solar activity based on neutron monitor records (Usoskin et al., 2011).

Figure 1 shows the comparison of mean ^{7}Be air activity concentration model results and measurements in latitudinal and vertical resolution. In the case of boundary layer observations (Fig. 1, left), the measured reference values are mean values from long-term time series, while high-altitude ^{7}Be observations rely on punctual measurements within aircraft or balloon surveys and thus show stronger scattering (Fig. 1, right). Different model results based on either the Masarik and Beer (2009) or the Usoskin and Kovaltsov (2008) production rate calculations differ by a factor of 2.40 on average (global average weighted with box sizes: 2.16). The differences show a latitudinal trend ranging from a factor of 1.7 (tropics) to 3.2 (polar latitudes) higher ^{7}Be model results in the case of the Usoskin and Kovaltsov (2008) production rate calculations. The model–measurement comparison reveals that the model quantitatively reproduces mean ^{7}Be air activity concentrations in the global boundary layer if the production rates from Usoskin and Kovaltsov (2008) are used. Model results based on the Masarik and Beer (2009) production rates clearly underestimate the observations by a factor of 2.4 on average. Having a look at the global distribution of atmospheric ^{7}Be, the model reproduces its main observed features: (i) a strong decrease from subtropical to mid- and high latitudes up to a factor of 5, (ii) a small ^{7}Be concentration in the tropics comparable to high (extra-polar) latitudes and, finally, (iii) a significant vertical gradient with ^{7}Be air concentrations decreasing over 2 orders of magnitude from mid-stratospheric to atmospheric boundary layers. The model underestimates ^{7}Be air concentrations in the northern mid-latitudes. This could be related to a deficient boundary layer–free troposphere (BL–FT) coupling or overestimated ^{7}Be deposition. So far, it is not possible to exactly validate the ^{7}Be air concentration in the free troposphere (see Fig. 1, right) and thus the BL–FT gradient. However, it is noticeable that the ^{7}Be model results for the southern free troposphere (not shown) are only 35 and 23 % (in the

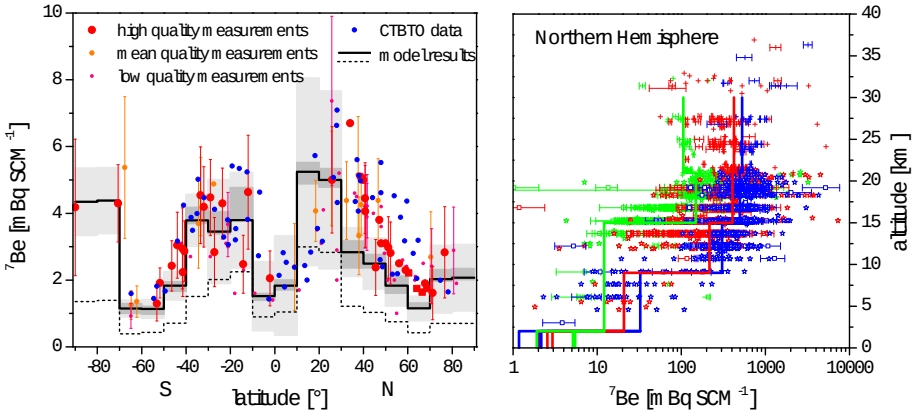

Figure 1. Model validation using global observations of the ^{7}Be activity air concentration (SCM is standard cubic meter). Left: model–measurement comparison of mean ^{7}Be activity concentrations in boundary layer air. Different sizes and colors of measurements (circles and squares) denote different quality of long-term mean values: high quality (time series longer than 10 years, > 10 months of data per year on average), mean quality (time series longer than 3 years, > 9 months of data per year on average) and low quality (shorter time series and literature data without details on sampling time); circles denote mean values and squares represent median values. Note that all elevated sites (> 1000 m a.s.l.) except South Pole station at 90° S are excluded. Blue symbols show unpublished data from the global CTBT monitoring system. These data allow for an independent model validation since sampling sites do not coincide with data used for model calibration. Model results are shown as black lines and grey shaded areas. Solid and dashed lines denote model results based on ^{7}Be production rate calculations by Usoskin and Kovaltsov (2008, solid line) and Masarik and Beer (2009, dashed line). The dark grey band indicates the model uncertainty from aerosol sink calibration. Light grey bars denote the standard deviation of the model results dominated by the seasonal cycle of the atmospheric concentrations. Model results encompass the mean of AD 1950–2000, whereas measurements represent various periods. Right: vertical distribution of ^{7}Be in the northern atmosphere according to US EML high-altitude sampling program data (symbols) and the GRACE model (lines) based on Usoskin and Kovaltsov (2008) production rates. Different colors denote different latitudinal bands according to the model resolution: polar (blue; 60–90° N), mid-latitude (red; 30–60° N) and tropical (green; 0–30° N). Different symbols represent the three different high-altitude sampling programs: stars (STAR DUST), squares (AIRSTREAM) and crosses (ASHCAN). Data: Kolb (1992); Durana et al. (1996); Megumi et al. (2000); Ioannidou et al. (2005); Wershofen and Arnold (2005); Kulan et al. (2006); Kulan (2007); Feely et al. (1981, 1985, 1988); Larsen and Sanderson (1990, 1991); Larsen et al. (1995); Feely et al. (1967); Leifer and Juzdan (1986); Leifer (1992); Chae et al. (2011); Elsässer et al. (2011); Leppänen et al. (2012); Doering (2007), and references therein.

case of polar and mid-latitudes) of the simulated concentrations in the respective northern free troposphere boxes. Different to the Southern Hemisphere, the model could thus have deficits in simulating the FT–BL vertical transport in the Northern Hemisphere. In the case of Antarctica, the ^{7}Be air activity concentration is significantly higher than in extrapolar high latitudes. Here, model results of the ice sheets are tuned to the mean observed ^{7}Be air activity concentration (see Sect. 2.1.2) which precludes model validation. Comparing our model results of the ^{10}Be air concentration (based on Kovaltsov and Usoskin (2010) production rates) to long-term observations from the coastal Antarctic Neumayer Station (Elsässer et al., 2011), our model only underestimates the measurements by 8 %. In the case of the Greenland ice sheet, ^{10}Be air concentration observations are restricted to 10 measurements covering the period June 1997–March 1998 (Stanzick, 2001). Here, model results exceed single month measurements by 30 % on average. However, due to the strong seasonal cycle (measured summer–winter ratio larger than 4) and the low data basis of 10 measurements, the ^{10}Be Greenland Summit model–measurement comparison is not very meaningful.

In addition to spatial characteristics of mean radionuclide air concentrations, model validation has to address their temporal variability. Given our climatological approach, evaluation of model performance has to address two features of ^{7}Be in the atmosphere: the dominant seasonal cycle and the 11-year solar production signal (see Koch and Mann (1996) for a global climatology of ^{7}Be measurements). Figure 2 shows long-term time series of ^{7}Be monitoring (i) at the Physikalisch-Technische Bundesanstalt (PTB) Braunschweig (Wershofen and Arnold, 2005), (ii) at the coastal Antarctic Neumayer Station (Elsässer et al., 2011) and (iii) at Greenland Summit Station (near the GISP2 drilling site; Dibb et al., 2007) compared to respective model results. Regarding the annual cycle, the model closely reproduces measured seasonal cycles in amplitude and phase at all three sites. However, in the case of the Greenland plateau, the model frequently underestimates the summer peak in the boundary layer ^{7}Be air activity concentration. In interpreting this results it is important to bear in mind that the model is forced to reproduce the seasonal cycle of the Greenland boundary layer ^{210}Pb (due to the calibration of BL–FT diffusive vertical air mass exchange, see Sect. S1.6). The mod-

els inability to reproduce the measured summer peak in the Greenland boundary layer ^{7}Be may thus originate from deficient simulation of ^{210}Pb (e.g., boundary layer transport from the Arctic basin to the Greenland ice sheet). Indeed, further model–measurement comparison of ^{7}Be seasonal cycles at globally distributed sites (see in the Supplement Sect. S1, Fig. S5) reveals that the model performance is very good in mid- and polar latitudes (no ^{210}Pb is involved in the model calibration). Major differences occur at low latitudes, only, where the model overestimates seasonal cycle amplitudes. Here, measurements in the tropics may be less representative for 10° boxes due to large spatial differences in tropical precipitation patterns (and thus local aerosol sinks, e.g., following monsoon patterns). On the multi-annual timescale, model–measurement comparison is difficult due to the overall low signal-to-noise ratio of the 11-year production signal. Indeed, the extraction of this production signal from measured time series is quite challenging (e.g., Koch and Mann, 1996; Aldahan et al., 2008; Elsässer et al., 2011). So far we eliminate the seasonal cycle of measurements and model results by using a simple Gaussian smoothing filter to investigate the model's ability to reproduce the production signal. Figure 2 reveals that the model clearly reproduces the cosmogenic production signal inherent to the time series even if the shape of the solar cycle somewhat differs. In the case of the nearly 50-year time series at the PTB Braunschweig, the measurements show an increasing trend which is missing in the model data (see Fig. 2a). Excluding measurement artifacts, possible explanations for this inconsistency are long-term climate effects (e.g., precipitation changes) which bias the atmospheric activity concentration and which are not considered in the observational-period model simulation.

In summary, the model validation shows that the model reproduces the climatology of ^{7}Be in the global atmosphere reasonably well. So far it is not possible to validate the model with ^{10}Be air concentration measurements since there are hardly any measurements available. However, given the model performance in terms of ^{7}Be, the model is likely also capable of simulating atmospheric ^{10}Be, since atmospheric concentrations of both (cosmogenic) radionuclides are governed by similar atmospheric production and sinks.

2.1.4 The ^{10}Be production signal in polar areas

Having a well-calibrated and validated model of the global atmospheric ^{10}Be transport at hand, we investigated the effect of atmospheric mixing on the ^{10}Be production signal inherent to polar ^{10}Be. To do so, we ran the model under constant conditions of present atmospheric transport and mean solar activity ($\Phi = 550$ MV following Masarik and Beer, 1999) but modulated the geomagnetic dipole field. Figure 3 shows the simulated effect of geomagnetic changes on ^{10}Be in the polar atmosphere and on the global mean atmospheric ^{10}Be concentration (i.e., the global atmospheric ^{10}Be inventory). It is obvious that the ^{10}Be air concentration in the case

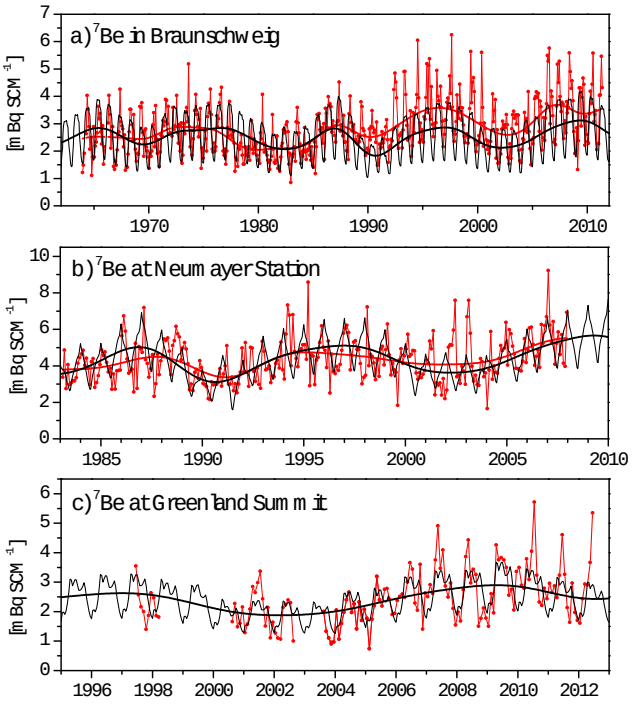

Figure 2. Comparison of measured (red circles) and modeled (black lines) ^{7}Be air concentration time series **(a)** in Braunschweig, **(b)** at coastal Antarctica (Neumayer Station) and **(c)** at Greenland Summit Station (near GISP2 drilling site). Model results (based on Usoskin and Kovaltsov (2008) production rate calculations) clearly match both features of the measurement time series, seasonal variations and decadal production changes. Note that the Greenland and Antarctic model results are tuned to the overall mean ^{7}Be air concentration. In the case of the Braunschweig (52° N) model–measurement comparison, the shown model results are 40–50° N.

of the Greenland and Antarctic ice sheets is less sensitive to geomagnetic activity than the global mean ^{10}Be air concentration. However, this polar damping effect depends on the production calculations applied: in the case of Kovaltsov and Usoskin (2010) production rate data, the geomagnetic signal in Greenland is up to 50 % lower than the global mean signal. Usage of the Masarik and Beer (2009) calculations only results in up to 22 % lower modulation of Greenland ^{10}Be. Certainly, this discrepancy is based on different geomagnetic modulation of the global mean ^{10}Be inventory: both production rate calculations differ in their latitudinal shape of the ^{10}Be production (i.e., their dependency of ^{10}Be production from cutoff rigidity) which implies a different geomagnetic modulation of the global mean ^{10}Be production. However, this difference is related to mid- and lower latitudes and there is obviously no difference at polar latitudes (no geomagnetic shielding, i.e., zero cutoff rigidity at polar latitudes). Indeed, our atmospheric transport model results show that – different to the global mean ^{10}Be – the geomagnetic modulation of polar ^{10}Be is similar in the case of the Masarik and Beer (2009) and Kovaltsov and Usoskin (2010) production

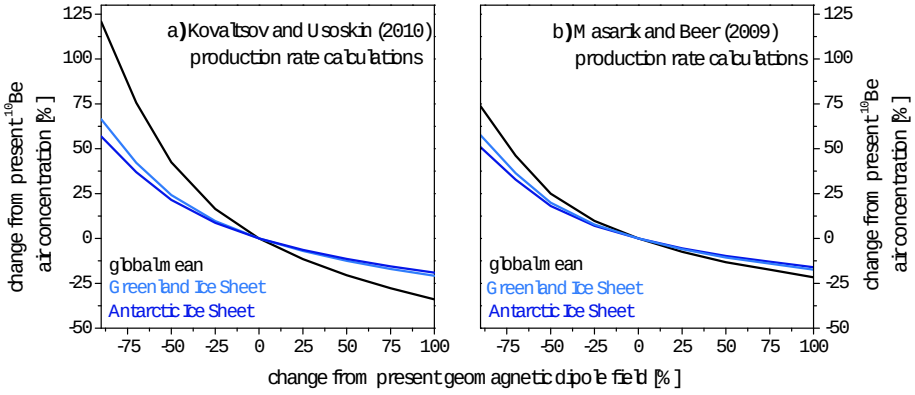

Figure 3. Modeled influence of the geomagnetic dipole field changes on atmospheric ^{10}Be illustrating the effect of atmospheric mixing. The left and right panel differ in the production rate calculations applied in the model simulations; **(a)** Kovaltsov and Usoskin (2010) or **(b)** Masarik and Beer (2009). Different lines show the global mean ^{10}Be air concentration (black) and local ^{10}Be air concentration on the Greenland (light blue) and Antarctic (deep blue) ice sheet. Solar activity is held constant at 550 MV. Note that the uncertainty of aerosol sink calibration (shown in Fig. 1) does not significantly influence the above results.

rates. The reason for this finding is that polar areas do not receive a globally mixed production signal. This atmospheric transport effect makes polar ice core ^{10}Be-based reconstructions of past geomagnetic activity less sensitive to the choice of ^{10}Be production rate calculations. This however does not hold for solar-activity-based production changes. Here, our model results show larger solar modulation of the polar ^{10}Be air concentration compared to the global mean (not shown). However, in comparison to the polar damping in the case of geomagnetic variations, this polar enhancement effect is less pronounced (9–16 and 12–17 % in the case of the Kovaltsov and Usoskin (2010) and Masarik and Beer (2009) production rates). In summary, our results reveal that polar latitudes do not receive a globally well-mixed atmospheric ^{10}Be production signal. In recent years, two GCM studies investigated the atmospheric footprint of the polar ^{10}Be deposition flux though achieved inconsistent results. Assuming that the polar ^{10}Be deposition is controlled by polar boundary layer ^{10}Be air concentration, our finding contradicts to GCM results from Heikkilä et al. (2009) (based on ECHAM5-HAM) but is in line with the results of Field et al. (2006) (using the GISS ModelE). The latter authors report on 20 % reduction of the geomagnetic modulation of polar ^{10}Be (based on Masarik and Beer (1999) production rates and in the case of a geomagnetic field decreased by 25 %). Using Masarik and Beer (2009) production rate calculations, our Greenland model simulations quantitatively confirm this result: 20–22 % lower geomagnetic modulation within the total range of analyzed global geomagnetic field changes.

2.2 Local air–firn transfer

Different and complex processes contribute to the hand over of atmospheric ^{10}Be into polar firn (see, e.g., Slinn, 1977), which still lack proper understanding. We therefore refrain from deploying a full physical process model but use a rather basic, measurement-calibrated air–firn transfer model approach to simulate the transfer of ^{10}Be from the polar boundary layer air into firn. In doing so we use observed spatial trends in polar ^{10}Be ice concentration to investigate its climate modulation. Across both the Greenland and the Antarctic ice sheets, climate conditions show large spatial gradients essentially between coastal areas and the remote interior. The ice sheets rise closely to the coast and mount up to 3 and 4 km (in the case of Greenland and Antarctica) entailing colder and dryer conditions at the polar plateaus. The observed difference in mean snow accumulation rates between coastal sites and the interior of the ice sheet amounts up to a factor of > 25 (Law Dome: > 60 cm year^{-1}, Smith et al., 2000; Vostok: 2.3 cm year^{-1}, Pourchet et al., 2003). These different climate conditions coincide with major differences in the mean ^{10}Be ice concentration of more than a factor of 8 (see Fig. 4). On the other hand, mean radionuclide air concentrations above the snowpack do not show large differences (e.g., Elsässer et al., 2011). The spatial gradient in the ^{10}Be ice concentration is thus governed by the processes delivering ^{10}Be from air to firn. Investigating this modulation of the ^{10}Be ice concentration by spatial change in local climate conditions therefore allows for investigation of the air–firn transfer and its climate variability.

2.2.1 Formulation of the basic air–firn transfer model

The model approach follows the basic idea that the total ^{10}Be deposition flux (J) consists of a wet and a dry deposition fraction. Using the net snow accumulation rate (A), the ^{10}Be ice concentration (c_{ice}) representative for a certain time inter-

val ($\Delta t = t_1 - t_0$) may be expressed as

$$c_{\mathrm{ice}}^{\Delta t} = \frac{\int_{t_0}^{t_1} [J_{\mathrm{dry}} + J_{\mathrm{wet}}] \mathrm{d}t}{\int_{t_0}^{t_1} A \mathrm{d}t}. \quad (1)$$

The ^{10}Be dry deposition flux depends on the ^{10}Be surface air concentration and the dry deposition velocity (v_{dry}). It comprises all deposition processes which are not related to precipitation. The wet deposition is the concentration of ^{10}Be in fresh snow times the precipitation rate (P). Assuming that both, the dry and wet deposition fractions are controlled by the same air mass, we may substitute the snow concentration using the scavenging ratio (ε – volume-based ratio between radionuclide concentration in snow and air) and get

$$c_{\mathrm{ice}}^{\Delta t} = \frac{\int_{t_0}^{t_1} [v_{\mathrm{dry}} \cdot c_{\mathrm{air}} + P \cdot c_{\mathrm{snow}}] \mathrm{d}t}{\int_{t_0}^{t_1} A \mathrm{d}t} = \frac{\int_{t_0}^{t_1} [v_{\mathrm{dry}} + P \cdot \varepsilon] \cdot c_{\mathrm{air}} \mathrm{d}t}{\int_{t_0}^{t_1} A \mathrm{d}t}. \quad (2)$$

On a well-chosen, climatological timescale we may assume the dry deposition velocity, the precipitation rate and the scavenging ratio as being a characteristic constant and get a first-order approximation of "climatologically averaged" terms

$$\overline{c}_{\mathrm{ice}} = \left(\frac{\overline{v}_{\mathrm{dry}} + \overline{P} \cdot \overline{\varepsilon}}{\overline{A}} \right) \cdot \overline{c}_{\mathrm{air}}. \quad (3)$$

The relation between precipitation rate and net accumulation rate depends on wind drift and evapo-sublimation. In polar areas, it is reasonable to assume the relation as being constant on a climatological timescale. The precipitation and net accumulation ratio may then be included into a modified scavenging ratio parameter ε^*. Since this parameter eludes a straightforward physical interpretation, we refrain from explicitly discriminating between ε and ε^* and get

$$\overline{c}_{\mathrm{ice}} = \left(\frac{\overline{v}_{\mathrm{dry}}}{\overline{A}} + \overline{\varepsilon} \right) \cdot \overline{c}_{\mathrm{air}}. \quad (4)$$

Following this basic air–firn transfer model, three main parameters govern the hand over of ^{10}Be from air to firn: the accumulation rate (A), the dry deposition velocity (v_{dry}) and the scavenging ratio (ε). While v_{dry} and ε cannot be measured directly, the relation between the measured mean ^{10}Be ice concentration and mean observed snow accumulation rates can be investigated in a straightforward way. To do so, we compile published mean ^{10}Be ice concentrations from different Antarctic sampling sites in addition to eight unpublished ^{10}Be firn core time series (Neumayer Hinterland, Kohnen Station, Berkner Island and Dome C). Figure 4a shows the compiled ^{10}Be ice concentration plotted against inverse mean snow accumulation rates at respective sites. Due to the involvement of different AMS laboratories in the ^{10}Be measurements, we recalibrated the different data using results from Nishiizumi et al. (2007) and Kubik and Christl (2010). Furthermore, we correct the effect of different temporal coverage and thus production variability of the ^{10}Be measurements (Fig. 4b; see Sect. S2 for details). The latter correction imposes revisions between −4.1 and 12.6 % to single data points. Eventually, Fig. 4b reveals that the mean ^{10}Be ice concentration at different Antarctic sites is well correlated to the inverse accumulation rate (correlation coefficient: 0.97). Hence, we conclude that spatial variation in the mean ^{10}Be ice concentration is driven by spatial accumulation changes at first order. The major differences between meteorological conditions at coastal and interior Antarctica seem to have less influence on the dry deposition velocity or aerosol scavenging. This finding allows for estimating the two missing parameters (v_{dry} and ε) of the basic model (Eq. 4) by investigating the relation between measured ^{10}Be ice concentration and corresponding snow accumulation rates.

2.2.2 Determination of model parameters

^{10}Be measurements within Greenland and Antarctic traverse surveys allow for more detailed investigations of the air–firn transfer processes. In comparison to the compilation of ^{10}Be literature data (Fig. 4), this approach allows for further reducing some uncertainty: (i) Measurements within each survey are conducted by only one AMS laboratory (see, e.g., Merchel et al., 2012 for comparability of different AMS facilities), (ii) all samples analyzed for the mean ^{10}Be ice concentrations broadly cover the same period of time and (iii) especially in the case of Antarctica, the spatial scale of single traverses is comparatively small (i.e., a few 100 km). It is thus very likely that all sampling sites are affected by comparable atmospheric transport conditions.

Surveys in Greenland and Antarctica were accomplished in cooperation with the Alfred Wegener Institute during 1990–1992 (Expedition Glaciologique Internationale au Groenland, EGIG), 1993–1995 (North Greenland Traverse, NGT) and 2006 (EDML upstream traverse). In addition, further snow-pit samples from the Antarctic Japanese–Swedish (JASE) traverse in 2007–2008 were analyzed for mean ^{10}Be ice concentrations. Details on the traverses and the ^{10}Be measurements are given in the Supplement (Sects. S2.3 and S.2.4). Figure 5 presents the results separated into Greenland and Antarctic measurements and compared to the linear trend of (mostly published) Antarctic-wide data (as shown in Fig. 4). Our measurements clearly confirm the finding of a linear relation between ^{10}Be ice concentration and the inverse accumulation rate. However, in both cases, the linear trend differs from the compilation of ^{10}Be measurements from the entire Antarctica: in the case of Greenland traverses, the slope of the linear fit falls below the Antarctic literature by a factor of 2.3. The ^{10}Be measurements within the Antarctic traverses reveal a factor of 1.9 stronger trend.

For the interpretation of these results, we use measured ^{10}Be air concentrations and apply Eq. (4) to the observed ^{10}Be ice concentration–accumulation rate relation. In

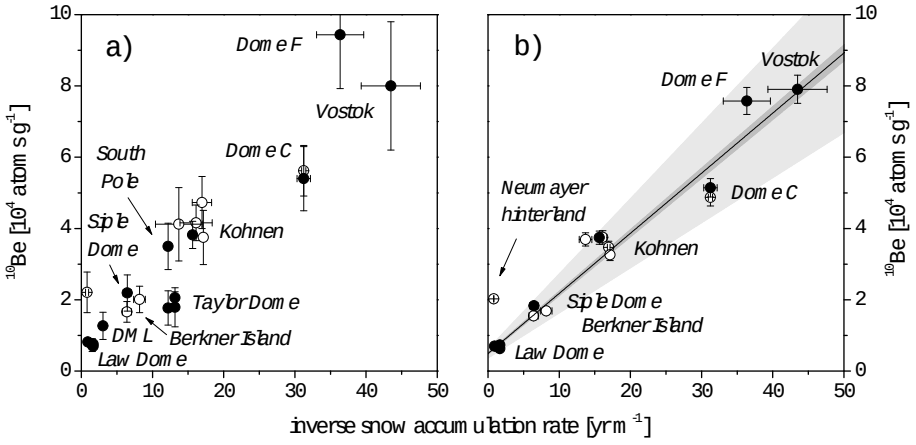

Figure 4. Mean ^{10}Be ice concentrations from various sites in Antarctica plotted against corresponding (inverse) snow accumulation rates (given in water equivalent). Filled dots refer to published data while open circles represent unpublished data. **(a)** Originally published values without any correction. Error bars denote the standard deviation of the respective time series. **(b)** Mean ^{10}Be concentrations corrected for different time coverage and AMS measurement standards (see Sect. 2.2 for details). Here, error bars show an average AMS uncertainty of 5 %. Note that, different to **(a)**, ^{10}Be data sets which lack information on the AMS calibration standard used for measurements are disregarded. The straight line denotes a linear fit to the data and the dark grey shaded area depicts the formal fitting error. Light grey shaded area is based on 25 % higher and lower slope (and y intercept) and covers all data points (except two outliers: 12 % of total number). Data: Raisbeck et al. (1990); Steig (1996); Aldahan et al. (1998); Smith et al. (2000); Nishiizumi and Finkel (2007); Horiuchi et al. (2008); Baroni et al. (2011); Pedro et al. (2012); Steinhilber et al. (2012). Further accumulation rate data: Jouzel et al. (1979); Sommer et al. (2000); Hamilton (2002); Pourchet et al. (2003); Oerter et al. (2004); Fernandoy et al. (2010).

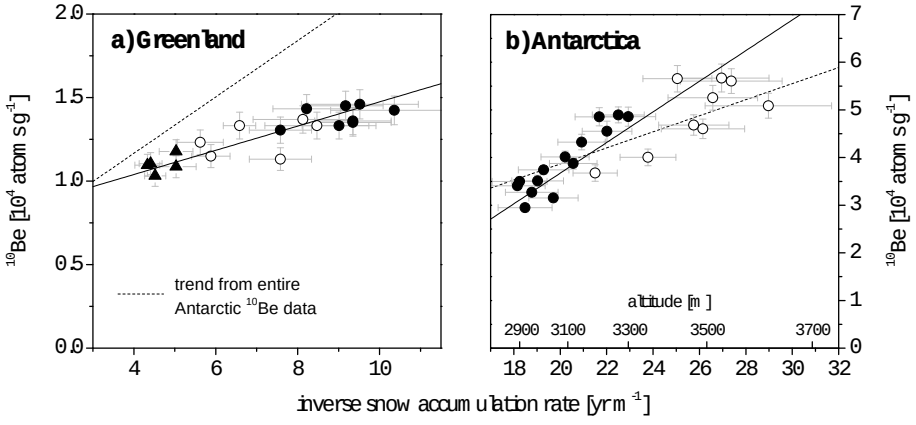

Figure 5. Spatial distribution of mean ^{10}Be firn concentrations measured within **(a)** Greenland and **(b)** Antarctic traverses. While solid lines denote linear fits to the above measurements, dashed lines depict the linear fit to Antarctic-wide data shown in Fig. 4. In both cases, Greenland and Antarctica, different symbols denote different traverse surveys: **(a)** NGT west (●), NGT east (▲), EGIG east (○). **(b)** Kohnen upstream (●), JASE (○) (see Sects. 2.3 and 2.4 for details).

the case of Antarctica, Elsässer et al. (2011) reported on 25 years of atmospheric ^{10}Be measurements at the coastal Neumayer station and found a mean air concentration of 4.6×10^4 atoms SCM^{-1} (standard cubic meter). In the case of Greenland, ^{10}Be air concentrations have to be deduced from 16 years of ^{7}Be measurements at the Greenland Summit Station (see Fig. 2) using a constant ^{10}Be / ^{7}Be ratio. The latter is based on 10 months of ^{10}Be measurements at Greenland Summit Station (Stanzick, 2001) resulting in a mean Greenland Summit ^{10}Be air concentration of $(2.4 \pm 0.4) \times 10^4$ atoms SCM^{-1} (uncertainty from ^{7}Be and ^{10}Be / ^{7}Be-based estimates). The difference in the mean ^{10}Be air concentration at Antarctic Neumayer and Greenland Summit sites is in line with the atmospheric ^{7}Be measurements at both sites which differ by a factor of 1.8 on average. Inserting these ^{10}Be air concentrations, our observed ^{10}Be ice concentrations and corresponding snow accumulation rates (Fig. 5) in our air–firn transfer model (Eq. 4) allows for estimating the missing model parameters (dry deposition and scavenging ratio) from a linear fit. In doing so we obtain

^{10}Be dry deposition velocities of $(0.10 \pm 0.02)\,\mathrm{cm\,s^{-1}}$ and $(0.22 \pm 0.03)\,\mathrm{cm\,s^{-1}}$ for Greenland and Antarctica, respectively. Thus, at first glance, our ^{10}Be measurements point to a stronger dry deposition velocity in Antarctica which may be caused by different glacio-meteorological conditions (i.e., non-precipitation-related processes like water vapor condensation on, and sublimation from the the snow surface). However, using the trend from the compilation of ^{10}Be measurements over the entire Antarctica (Fig. 4) within the model, the resulting dry deposition of $(0.116 \pm 0.003)\,\mathrm{cm\,s^{-1}}$ meets the Greenland results surprisingly well. Different reasons may account for the mismatch between the local Antarctic traverses around Kohnen Station and the entire Antarctic data compilation. At first the assumption of a constant ^{10}Be air concentration over the entire Antarctica is a rough oversimplification and regional trends in atmospheric ^{10}Be could affect the results of the large-scale data compilation. On the other hand, the determination of mean accumulation rates in dry Antarctic conditions is challenging (see Sect. S2.4) and the Antarctic-wide data compilation thus allows for a more robust estimation of accumulation rate trends. Within this study we focus on Greenland model results and use an overall dry deposition velocity of $0.1\,\mathrm{cm\,s^{-1}}$. In the case of model results for Antarctica, both ongoing measurements of atmospheric ^{10}Be at the high Antarctic plateau and ongoing extension of ^{10}Be ice concentration measurements to very low accumulation sites will provide further constraints on the model parameters. The second decisive parameter for the ^{10}Be air–firn transfer is the volume-based ratio between ^{10}Be air and firn concentration (scavenging ratio). Applying Eq. (4) to the spatial ^{10}Be trends gives a ratio of $(3.1 \pm 0.6) \times 10^5$ [atoms $\mathrm{m_{air}^{-3}}$ / atoms $\mathrm{m_{snow}^{-3}}$] for Greenland which corresponds to a ^{10}Be concentration of $(7.5 \pm 0.7) \times 10^3\,[\mathrm{atom\,g^{-1}}]$ in fresh fallen snow. Here, the model applied to Antarctic literature data gives a factor of 2.8 lower scavenging ratio. Again the generally dryer and colder conditions may be responsible for this difference.

2.2.3 Dry versus wet deposition at Greenland Summit

The site-specific ratio of dry versus wet deposition of ^{10}Be is a valuable parameter for the interpretation of ^{10}Be ice core records. Generally speaking, in case of dominating wet deposition processes, the ^{10}Be ice concentration is less influenced by accumulation rate changes making the ^{10}Be ice concentration a primary reference for atmospheric ^{10}Be production changes (see, e.g., the detailed discussion in Alley et al., 1995). On the other hand, dominating dry deposition implicates larger influence of snow accumulation variability. Here, the interpretation of the ^{10}Be deposition flux (derived from ^{10}Be ice core records) in terms of cosmogenic production changes is common practice (e.g., Muscheler et al., 2004, 2005). Our air–firn transfer model results indicate that wet deposition processes dominate the Greenland Summit ^{10}Be ice concentration under present conditions (mean snow accumulation rate at GRIP drilling site: $0.21\,\mathrm{m\,yr^{-1}}$ water equivalent; Johnsen et al., 1992) and dry deposition only accounts for 32 % of the total ^{10}Be deposition. Assuming an overall mean Greenland precipitation rate of $0.3\,\mathrm{m\,yr^{-1}}$ (Bales et al., 2001), this value is slightly lower for the entire Greenland (24 %) and the ^{10}Be sink in the Greenland ice sheet model box (see Sect. 2.1). Using ^{210}Pb instead of ^{10}Be measurements results in a similar Greenland ice sheet dry to total deposition ratio of 30 % (Stanzick, 2001). It is worth mentioning that this figure holds as well for the (sub-micron) non-sea-salt sulfate distribution in central Greenland investigated by Fischer and Wagenbach (1996). Using the same deposition model approach they arrived at a dry deposition flux fraction of 37 % for this species which was consistent with the direct observations reported by Bergin et al. (1995) from Summit.

Global circulation model results (Field et al., 2006; Heikkilä et al., 2008a) report a larger impact of wet deposition in the case of Greenland (i.e., dry deposition less than 10 %). So far, this mismatch remains unexplained. However, regarding the GCM results from Heikkilä et al. (2008a), overestimated wet deposition might contribute to their significantly underestimated Antarctic ^{7}Be activity air concentration. Finally, in terms of interpreting ^{10}Be ice core records, the ratio of dry to total deposition flux is most likely not constant under climate change. Investigating temporal changes in ^{10}Be deposition at Greenland Summit, Alley et al. (1995) found that any variations in the dry deposition velocity and scavenging ratio have been small. We may thus assume linear scaling of wet deposition with accumulation rates to investigate the effect of climate change on the ratio of dry to total deposition. Using reconstructed variations of the GRIP snow accumulation rate (see also Fig. 7a) as model input we find that the ^{10}Be air–firn transfer at Greenland Summit is dominated by dry deposition (ratio of dry to total deposition up to 65 %) during the last glacial stadials.

Alley et al. (1995) regressed ^{10}Be (among other aerosol species) from the Summit GISP2 core versus accumulation rate (using the same deposition model approach as the present study). The authors inferred the relative change in the atmospheric ^{10}Be load between late glacial (cold) stadials and (warm) interstadials. Here, the temporal changes of the deposition regime climatology have been deployed instead of spatial changes as done in the present study. Their finding limits the respective cold / warm ^{10}Be ratio to less than 1.5 with the most likely ratio around 1.2.

2.3 Looking into the past: model simulations on the glacial–interglacial timescale

Coupling the model of the global atmosphere (Sect. 2.1) to the air–firn transfer model (Sect. 2.2) allows for quantitative simulations of the ^{10}Be ice concentration in polar areas. Model-based investigations of ^{10}Be ice core records additionally require adequate input data driving the time depen-

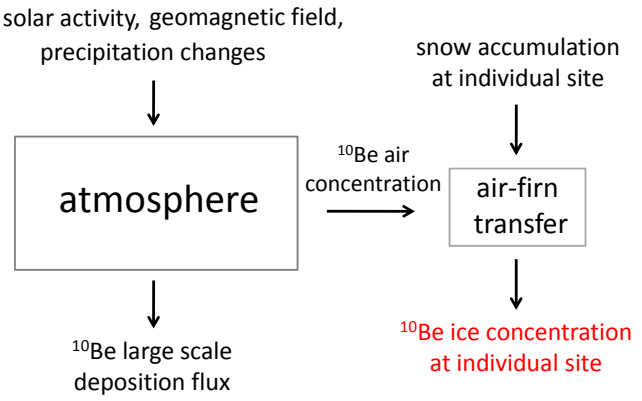

Figure 6. Sketch of our basic model approach to simulate ^{10}Be ice core records on the glacial–interglacial timescale. The model setup of the atmosphere is presented in Sect. 2.1, whereas the air–firn transfer model is put forward in Sect. 2.2. Model input records are discussed in Sect. 2.3.

dency of the model results. Both, variations of ^{10}Be production and changes in climate conditions have to be taken into account and will be addressed subsequently. The final model setup for the investigation of ^{10}Be ice core records is summarized in a basic sketch shown in Fig. 6.

2.3.1 Production variability

A fundamental process influencing the temporal variability of ice core ^{10}Be is its atmospheric production rate. Basically, solar activity, changes in the geomagnetic field strength as well as variations in the galactic cosmic ray flux modulate the atmospheric production of ^{10}Be. However, only geomagnetic variations have been clearly proven to impose multi-millennial variations on the production rate of cosmogenic radionuclides. Therefore, focusing on the glacial–interglacial timescale, we restrict changes of the ^{10}Be production to variations in the geomagnetic dipole field. We choose the high-resolution geomagnetic reconstruction from Laj et al. (2004) which is based on a selection of 24 high-accumulation marine sediment records (GLOPIS-75). The record is converted from the GISP2 timescale to the most up-to-date Greenland ice-core chronology (GICC05modelext timescale), by using partly unpublished match points between the NorthGRIP, GRIP and GISP2 ice cores (Seierstad et al., 2014) (see Fig. 7b and Sect. S3.1). Since geomagnetic modulation of polar ^{10}Be is not very sensitive to the choice of different production rate calculations (see Sect. 2.1.4), we use the production rate calculations of Kovaltsov and Usoskin (2010) throughout. Solar activity is kept constant at a mean value of 550 MV (Masarik and Beer, 1999). Indeed, solar activity might also show variation on timescales longer than the well-known multi-centennial period. However, (^{10}Be-independent) ^{14}C-based reconstructions are so far restricted to the Holocene period. Here, differences in ^{10}Be- and ^{14}C-based reconstructions leave the magnitude of multi-millennial variations of solar activity subject to debate (Vonmoos et al., 2006).

2.3.2 Climate variability

It is important to highlight that our model approach essentially differs from global climate model attempts and does not allow for implicit climate modulation of atmospheric ^{10}Be by, e.g., varying the atmospheric concentration of greenhouse gases. However, we may explicitly vary processes which have been proven to (i) influence the ^{10}Be ice concentration and (ii) vary on the glacial–interglacial timescale. So far, we restrict climate modulation to precipitation/snow accumulation changes which are comparatively well known. Precipitation governs both, the tropospheric residence time of ^{10}Be (i.e., the ^{10}Be deposition; Heikkilä and Smith, 2013) and the local ^{10}Be air–firn transfer (Stanzick, 2001). Recent GCM model results by Heikkilä et al. (2013) indicate that changes in the ^{10}Be deposition are also consistent with precipitation changes under different climate conditions. However, the authors find additional atmospheric circulation changes influencing the ^{10}Be air concentration (mainly in higher atmospheric layers). Future applications of the model setup presented here may easily include further processes of climate variability (as, e.g., modulation of atmospheric air mass transport). However, for this study, changes in the atmospheric circulation or air–firn parameterization (i.e., dry deposition velocity and aerosol scavenging) are not taken into account. We are well aware that this simplistic approach is a rough oversimplification. However, sensitivity studies on atmospheric transport and deposition indicate that present-day polar boundary layer ^{10}Be is quite robust against global-scale circulation changes (Elsässer, 2013). On the contrary, these studies indicate that polar boundary layer ^{10}Be is very sensitive to local polar air mass transport (i.e., boundary layer–free troposphere coupling). This is reasonable given the radionuclide concentration in the (polar) free troposphere exceeding common (polar) boundary layer concentrations by an order of magnitude (see Fig. 1 for ^{7}Be). Still, processes of ice sheet boundary layer atmospheric transport are not understood sufficiently and global circulation models have issues with reproducing polar ^{7}Be sufficiently well. We are thus not sure if usage of complex climate models would significantly improve simulations of local conditions on the ice sheets.

For our model study, model input records of past precipitation changes are predicated on ice-core-based reconstructions of snow accumulation, which clearly show that glacial precipitation and snow accumulation rates (in polar areas) have been significantly lower than today (e.g., Dahl-Jensen et al., 1993). However, these investigations concern local conditions while estimations of regional or global-scale changes in precipitation patterns are difficult. Paleoclimate models differ in their results on glacial–interglacial changes in amount and latitudinal distribution of precipitation. However, sum-

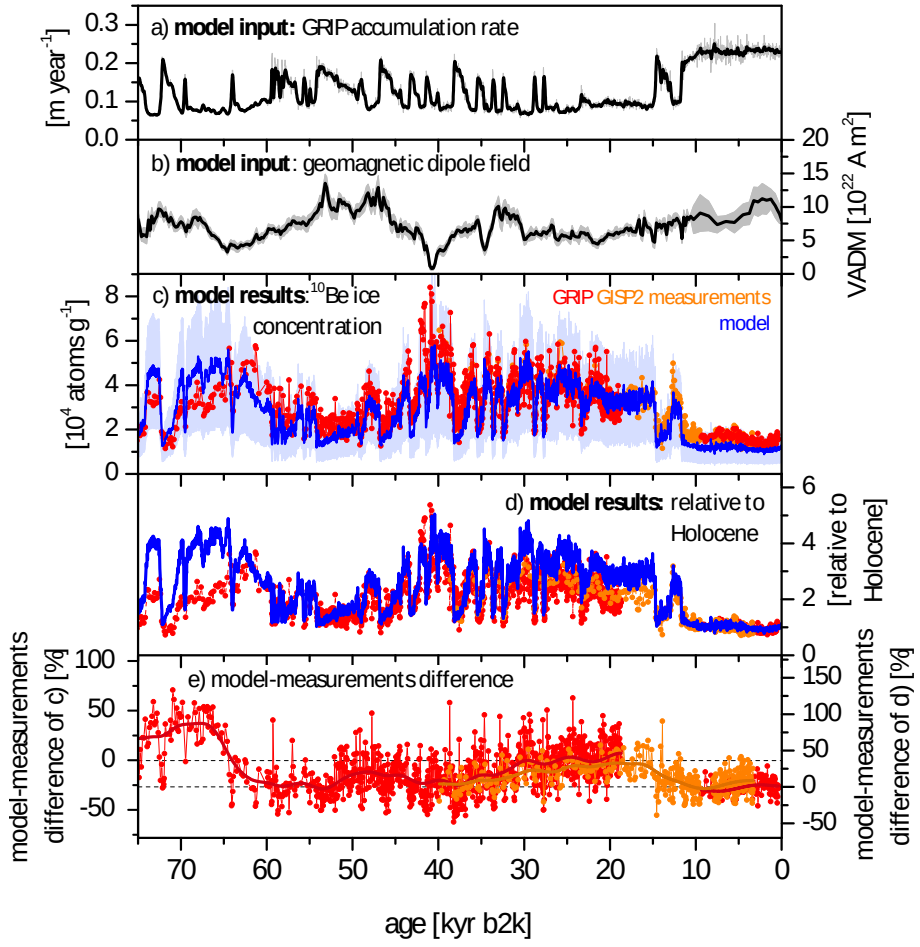

Figure 7. Model results of the ^{10}Be ice concentration at Greenland Summit compared to respective ice core measurements. **(a)** and **(b)** show the model input data driving the temporal variation of the model results: GRIP accumulation and geomagnetic dipole field strength (Laj et al., 2004) both on the GICC05modelext timescale (see text for details). **(c)** shows the ^{10}Be model results (blue) compared to GRIP (red dots; Yiou et al.,1997; Wagner et al., 2001a; Muscheler et al., 2004) and GISP2 (orange dots; Finkel and Nishiizumi, 1997) measurements. The blue band denotes the original model results including the seasonal cycle. Thick blue lines show yearly mean model results. **(d)** shows model results and measurements normalized to the Holocene period. Model–measurement differences of **(c)** and **(d)** are shown in **(e)** relative to measurements. Here, thick lines denote Gaussian smoothing which dampens 2000-year oscillations to 0.1 %.

marizing common findings, model inter-comparison projects report on glacial drying being the largest over the ice sheets and sea ice (Braconnot et al., 2007). Ice-core-based reconstructions of precipitation rates may thus give an upper limit to glacial–interglacial differences. For our model study, we use a revised version of the GRIP snow accumulation rate (Fig. 7a) based on the GICC05modelext timescale (see Sect. S3.1). We use two different scenarios for adopting the ice-core-based precipitation changes to the hemispheric precipitation pattern: (i) Precipitation in the Greenland ice sheet box modulated by relative changes of the GRIP accumulation rate, but constant precipitation rates in the residual northern hemispheric boxes. (ii) precipitation in the entire high latitudes boxes (60–90° N) modulated by relative changes of the GRIP accumulation rate but constant precipitation rates in mid- and low latitudinal boxes (0–60° N). However, ^{10}Be model results of both scenarios do not differ by more than 2 %. This finding is expected given the model setup for the Greenland ice sheet: the diffusive air mass transport between the Greenland boundary layer air mass and the surrounding Arctic basin boundary layer is inhibited (see Sect. S1.6). Radionuclides in the Greenland boundary layer air are supplied from the free polar troposphere. Since the inventory of radionuclides in the free polar troposphere is hardly modulated by polar boundary layer sink strength, ice sheet boundary layer ^{10}Be is not very sensitive to precipitation changes outside the ice sheet box.

3 Results for Greenland Summit

Finally, we present forward model results for the Greenland Summit ^{10}Be ice concentration covering the last 75 kyr. Since the GRIP and GISP2 ^{10}Be ice core profiles are widely used in different studies (e.g., Muscheler et al., 2004, 2005; Köhler et al., 2006), model–measurement comparisons of the two Greenland Summit ice core records is especially informative. However, for future investigations, model simulations can be easily expanded for different sampling sites in Greenland and Antarctica, if site-specific changes of snow accumulation are known sufficiently well.

3.1 Results

Modeled Greenland Summit ^{10}Be ice concentration time series is shown in Fig. 7 together with the measured profiles from the GRIP and GISP2 ice cores (Finkel and Nishiizumi, 1997; Yiou et al., 1997; Wagner et al., 2001a; Muscheler et al., 2004) and the time-dependent model input data. The measurements have been corrected for ^{10}Be decay (3.8 % at most for the last 75 kyr), revised AMS calibration (Nishiizumi et al., 2007) and sample processing effects (see Sect. S3.2 for details). Neither the GRIP nor the GISP2 ^{10}Be measurements cover the observational period. However, comparing our model results to firn core ^{10}Be measurements from the GRIP drilling site, we find that the model only underestimates the recent ^{10}Be ice concentration by 4 % (Heikkilä et al., 2008b) and 6 % (Stanzick, 1996) (firn core accumulation rates taken from respective studies and solar activity taken from Usoskin et al., 2011). Due to lack of measurements, it is not possible to directly validate the simulated ^{10}Be air concentration at Greenland Summit (see Sect. 2.1.3). However, we may specify the model–measurement deviation of the air–firn transfer model (which is the difference of observed ^{10}Be ice concentration at a single site to the overall linear fit in Fig. 5). In the case of both Greenland Summit firn cores, the overall model–measurement divergence is dominated by this air–firn transfer model divergence (4 and 5 %) which points to a good overall performance of the atmospheric model in reproducing the ^{10}Be air concentration in Greenland. In the case of the entire Holocene period, absolute model–measurement differences are larger (see Fig. 7c and e) with the model underestimating observed ^{10}Be ice concentrations by 27 % (mean GRIP; median: 27 %; interquartile range: 12 %) and 24 % (mean GISP2; median: 24 %; inter-quartile range: 14 %).

Focusing on glacial–interglacial changes of the ^{10}Be ice concentration we compare our model results to the observed ice core records on a normalized scale. In doing so we use the major part of the Holocene period where GRIP ^{10}Be measurements are available (9361–355 yr b2k) as reference and divide the time series by this "Holocene mean". In the case of the GISP2 record, measurements do not cover this whole period and we use the GRIP Holocene ^{10}Be ice concentration for normalization. Figure 7d reveals that the model captures both dominant features of the measured ^{10}Be ice core records: (i) a factor of 2–3 rise in the ^{10}Be ice concentration from Holocene to glacial periods and (ii) the millennial-scale variability during the last glacial period related to Dansgaard–Oeschger events. During the glacial period, the model (normalized to the Holocene) overestimates the GRIP and GISP2 data by 19 % (mean: 22 %, inter-quartile range: 39 %) on average. However, model–measurement residuals are not randomly distributed around a constant offset but show some significant low-frequency oscillations (see Fig. 7e, right axis). The most prominent model–measurement difference occurs during the (62–75 kyr) b2k period, where the model (normalized to the Holocene) overestimates measured ^{10}Be ice concentrations by 65 % on average (median: 74 %, interquartile range: 61 %). Here, smoothed model–measurement differences come up to 87 % of the observed mean Holocene ^{10}Be ice concentration. Moreover, the model significantly overestimates the observations in 12–37 kyr b2k (average: 31 % GRIP, 20 % GISP2) and 43–52 kyr b2k (average: 15 % GRIP). On the other hand, the mean model–measurement differences are low during 37–43 and 52–62 kyr b2k.

3.2 Discussion

Given the large variations inherent to the ^{10}Be ice concentration our basic model reproduces the largest part of the observed ^{10}Be ice core records. It is of major interest that the model–measurement differences do not show a constant offset over the entire glacial period. In addition, correlation analysis with the GRIP δ^{18}O record (primary reference for climate variability; Johnsen et al., 1997) reveals that the model accounts for the major part of climate modulation: while the measured ^{10}Be ice concentration shows a significant negative correlation (GRIP: $r = -0.75$; GISP2: $r = -0.90$), model–measurement differences (as shown in Fig. 7e) are less correlated to the stable isotopes record (GRIP: $r = -0.38$; GISP2: $r = -0.43$). This finding does also hold for the glacial period, indicating that the model explains a major fraction of fast glacial climate variations (related to Dansgaard–Oeschger events). However, the multi-millennial trends in the model–measurement differences (up to 87 % of the Holocene mean) call for a detailed discussion of their likely origin. Deficient model input records as well as unconsidered climate variations could basically account for this model–measurement mismatch.

Analyzing the sensitivity of ice core ^{10}Be to different processes, we firstly investigate the share of the different model input records in the simulated ^{10}Be variability. Figure 8 shows that the major part of the ^{10}Be variations is driven by climate changes (i.e., precipitation and snow accumulation changes) while geomagnetic modulation is less decisive. Regarding the latter, only the Laschamp geomagnetic excursion around 42 kyr induces a prominent ^{10}Be peak up to +73 %

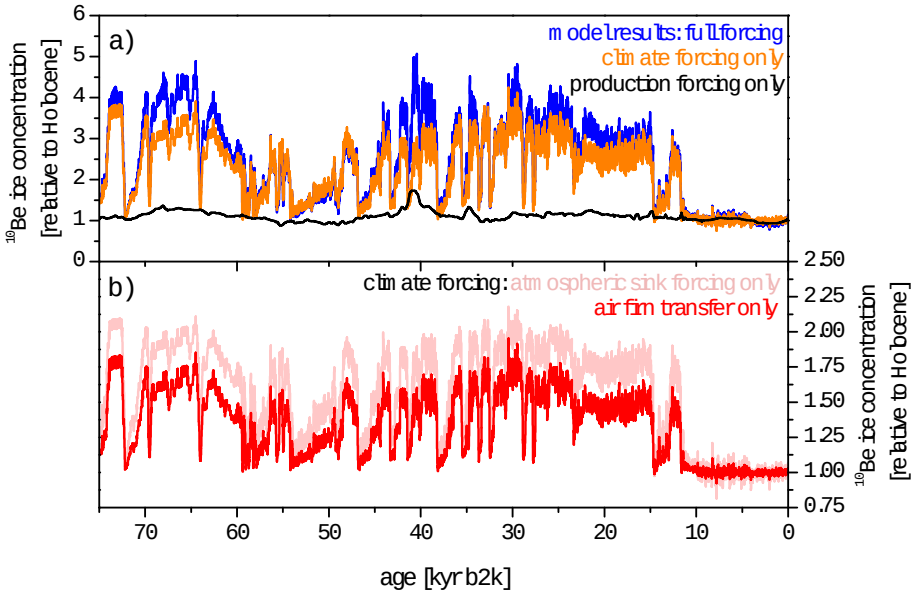

Figure 8. Sensitivity of Greenland Summit ^{10}Be ice concentration model results with respect to different influencing processes. **(a)** Model results using constant geomagnetic activity (climate forcing only, orange) compared to model results with constant precipitation/snow accumulation rate (production forcing only, black) and full forcing (blue). **(b)** Breakdown of climate modulation into air–firn transfer (red) and atmospheric sink strength (light red).

of the overall Holocene mean ^{10}Be ice concentration. Apart from that, the geomagnetic modulation is generally lower than 36 % which is comparable to the model–measurement differences. Indeed, focusing on the (12–37) kyr b2k period, the geomagnetic dipole record applied in the model simulations (GLOPIS75, Laj et al., 2004) would need average revision by +222 % to adapt the (normalized to Holocene) model results to the measurements. This would result in a geomagnetic dipole moment which would exceed the mean Holocene value. It is thus very unlikely that geomagnetic changes account for a major part of the model–measurement differences. The atmospheric production of ^{10}Be could however also hold multi-millennial modulation due to solar activity. Though not varied in the model simulations, long-term trends in solar activity could thus contribute to the model–measurement differences (see, e.g., Vonmoos et al. (2006) for Holocene multi-millennial variations reconstructed from ^{14}C and ^{10}Be). Indeed our model results show that the polar ^{10}Be ice concentration is more sensitive to solar activity than the global mean ^{10}Be air concentration (see Sect. 2.1.4). However, regarding the (12–37) kyr b2k period, the (so far constant) solar activity would require average increase by +72 % to explain the (relative to Holocene) model–measurement differences. We may thus conclude that production changes are not responsible for a large share of the model shortcomings. This does not hold for climate modulation of the ^{10}Be ice concentration. Here, precipitation and snow accumulation changes modulate the simulated ^{10}Be ice concentration up to 400 % (Fig. 8a). The applied GRIP snow accumulation record would require much less revision to account for the model–measurement differences (i.e., +30 % on average during (12–37) kyr b2k). This larger sensitivity of the ^{10}Be ice concentration is based on two different effects: Lower accumulation rates during the glacial period result in both, a lower Greenland boundary layer atmospheric ^{10}Be sink (and thus higher ^{10}Be air concentration) and a larger ratio of the (local) ^{10}Be ice concentration to the ^{10}Be air concentration. Investigating both effects, we find that the latter falls below the impact of a changing Greenland atmospheric sink strength (Fig. 8b). This finding is, however, decisively based on the assumption that the atmospheric ^{10}Be sink in the entire Greenland resembles the local ^{10}Be air–firn transfer with respect to dry deposition, aerosol scavenging and relative GRIP accumulation rate changes. Moreover, a major assumption is linear scaling of the ^{10}Be deposition flux with precipitation (i.e., constant scavenging efficiency as e.g., found by Alley et al., 1995). Assuming, i.e., larger aerosol scavenging efficiency during the glacial period would result not only in lower Greenland ^{10}Be air concentration (larger sink strength) but also in stronger air–firn transfer flux. This twofold effect entails a low sensitivity of the ^{10}Be ice concentration to changes in the dry deposition velocity and scavenging ratio. In addition, unconsidered changes of atmospheric transport could likely have an additional share in the model–measurement differences. Our model results predict a free polar troposphere ^{10}Be air concentration which is a factor of 15 higher than in the Greenland ice sheet boundary layer (see also Fig. 1 for ^{7}Be measurements). Vertical atmospheric mixing is thus a decisive process influencing the ^{10}Be air and ice concentration. Indeed the model–measurement dif-

Table 1. Required revision of model input records to account for the (normalized to Holocene) model–measurement differences during (12–37) kyr b2k (30 % of the observed Holocene mean, combined GRIP–GISP2 record). Note that, different to the geomagnetic dipole strength and the Greenland snow accumulation rate, the original model input parameters for solar activity and the diffusive BL–FT do not vary on a multi-annual scale.

Parameter	Revision during (12–37) kyr b2k to explain model measurement differences
Geomagnetic dipole field	+222 %
Solar activity	+72 %
Snow accumulation rate	+28 %
Diffusive BL–FT coupling	−26 %

ferences during (12–37) kyr b2k could be explained by an average reduction of the diffusive boundary layer–free troposphere coupling by only 26 %. It is thus very likely that model–measurement differences are related to climate variability (see Table 1 for a summary of the sensitivity studies). Adequate knowledge of changes in ^{10}Be atmospheric transport and deposition is thus a fundamental requirement for ^{10}Be ice-core-based reconstruction of geomagnetic and solar activity.

4 Summary and outlook

We present a climatological model approach of the ^{10}Be ice concentration which allows for the first quantitative (sub-annual-resolution) simulations up to the glacial–interglacial timescale. The model thus satisfies the demand for an easy-to-use tool to support the interpretation of ^{10}Be ice core measurements on long timescales. In specifically configuring the model setup for ice core ^{10}Be, we coupled a (coarse grid) model of the global atmosphere to a basic, measurement-supported air–firn transfer model. In addition to polar measurements of ^{10}Be, comprehensive observational data of different (cosmogenic, anthropogenic and terrigenic) short-lived aerosol-borne radionuclides on the global and polar scale have been applied for model calibration and validation.

Investigating the production signal of ^{10}Be in polar areas, our model results show that ^{10}Be is not well mixed in the global atmosphere. In comparison to the global mean atmospheric ^{10}Be concentration, polar ^{10}Be is less modulated by changes of the geomagnetic dipole field (but more sensitive to solar activity). In the case of Greenland, the amount of this polar damping of the geomagnetic modulation of ^{10}Be comes up to 50 %, but significantly depends on the production rate calculations applied. Indeed, calculations based eather on the Masarik and Beer (2009) or on the Kovaltsov and Usoskin (2010) production rates reveal significantly different geomagnetic modulation of the global mean ^{10}Be air concentration. However, model results using the different production rate calculations coincide in the geomagnetic modulation of ^{10}Be at polar latitudes. Reconstructions of past geomagnetic activity based on ice core ^{10}Be are therefore not very sensitive to the production rate calculations applied. However, this does not hold for solar-activity-induced changes of polar ^{10}Be.

On the glacial–interglacial timescale, observed Greenland ^{10}Be ice core records show large variation of up to 400 % from the overall Holocene mean. Applying the model to simulate the Greenland Summit (GRIP and GISP2) ^{10}Be ice core records, we could reproduce the major portion of these ^{10}Be ice concentration changes. However, multi-millennial trends in the (normalized to Holocene) model–measurement residuals come up to 87 % and call for further analysis. We investigated potential contributions to the model–measurement mismatch within a sensitivity study: focusing on the (12–37 kyr) b2k (before the year AD 2000) period, strong revision of the geomagnetic (+222 %) or solar (+72 %) activity would be required to explain the model–measurement difference of 30 % on average. In contrast, the ^{10}Be ice concentration is much more sensitive to the Greenland snow accumulation rates or atmospheric boundary layer–free troposphere mixing (revision of +28 or −26 % to account for the model–measurement differences). We thus conclude that model–measurement differences are very likely related to climate variability. On pre-Holocene timescales, ^{10}Be-based reconstruction of solar and geomagnetic activity thus requires detailed knowledge on climate-induced changes of the ^{10}Be ice concentration.

The model presented here has large potential to support interpretation of measured ^{10}Be ice core records within future studies. At first the handiness of the model setup allows for further sensitivity studies on the effect of prescribed, climate-related changes of ^{10}Be transport and deposition (e.g., less/more stratosphere–troposphere exchange) on ice core ^{10}Be. Second, model applications on very different timescales (sub-annual to several 100 kyr) enable direct comparison and combination of different ^{10}Be ice core records as well as interpolation of data gaps. Finally, the comparatively simple model setup allows for model inversion and thus direct reconstruction of production- and climate-related parameters from ^{10}Be ice core records.

The Supplement related to this article is available online at doi:10.5194/cp-11-115-2015-supplement.

Acknowledgements. The authors would like to thank the Preparatory Commission for the Comprehensive nuclear-Test-Ban Treaty Organisation (CTBTO) for providing limited vDEC access to unique global atmospheric ^{7}Be measurements. The views expressed within this publication are those of the authors and do not

necessarily reflect the view of CTBTO Preparatory Commission. Special thanks go to Carlo Laj (LSCE, Gif-sur-Yvette) for providing the GLOPIS-75 geomagnetic reconstruction data as well as Margareta Hansson (Stockholm University) for JASE snow-pit samples. The work was partly funded by the German Science Foundation (DFG) within research grant DFG LE 1198/4-1.

Edited by: V. Rath

References

Adler, R. F., Huffman, G. J., Chang, A., Ferraro, R., Xie, P. P., Janowiak, J., Rudolf, B., Schneider, U., Curtis, S., Bolvin, D., Gruber, A., Susskind, J., Arkin, P., and Nelkin, E.: The version-2 global precipitation climatology project (GPCP) monthly precipitation analysis (1979–present), J. Hydrometeorol., 4, 1147–1167, 2003.

Aldahan, A., Possnert, G., Johnsen, S. J., Clausen, H. B., Isaksson, E., Karlen, W., and Hansson, M.: Sixty year ^{10}Be record from Greenland and Antarctica, P. Indian. A.S.-Earth, 107, 139–147, 1998.

Aldahan, A., Hedfors, J., Possnert, G., Kulan, A., Berggren, A.-M., and Söderström, C.: Atmospheric impact on beryllium isotopes as solar activity proxy, Geophys. Res. Lett., 35, L21812, doi:10.1029/2008GL035189, 2008.

Alley, R. B., Finkel, R. C., Nishiizumi, K., Anandakrishnan, S., Shuman, C. A., Mershon, G. R., Zielinski, G. A., and Mayewski, P. A.: Changes in continental and sea-salt atmospheric loadings in central Greenland during the most recent deglaciation: model-based estimates, J. Glaciol., 41, 503–514, 1995.

Arthern, R. J., Winebrenner, D. P., and Vaughan, D. G.: Antarctic snow accumulation mapped using polarization of 4.3-cm wavelength microwave emission, J. Geophys. Res.-Atmos., 111, D06107, doi:10.1029/2004JD005667, 2006.

Bales, R. C., McConnell, J. R., Mosley-Thompson, E., and Csatho, B.: Accumulation over the Greenland ice sheet from historical and recent records, J. Geophys. Res., 106, 33813–33825, 2001.

Bard, E., Raisbeck, G. M., Yiou, F., and Jouzel, J.: Solar modulation of cosmogenic nuclide production over the last millennium: comparison between ^{14}C and ^{10}Be records, Earth Planet. Sc. Lett., 150, 453–462, 1997.

Baroni, M., Bard, E., Petit, J. R., Magand, O., and Bourles, D.: Volcanic and solar activity, and atmospheric circulation influences on cosmogenic ^{10}Be fallout at Vostok and Concordia (Antarctica) over the last 60 years, Geochim. Cosmochim. Ac., 75, 7132–7145, 2011.

Beer, J., Oeschger, H., Finkel, R. C., Castagnoli, G. C., Bonino, G., Attolini, M. R., and Galli, M.: Accelerator measurements of ^{10}Be: The 11 year solar cycle from 1180–1800 A.D., Nucl. Instrum. Meth. B, 10–11, 415–418, 1985.

Beer, J., Siegenthaler, U., Bonani, G., Finkel, R. C., Oeschger, H., Suter, M., and Wölfli, W.: Information on past solar activity and geomagnetism from ^{10}Be in the Camp Century ice core, Nature, 331, 675–679, 1988.

Bergin, M. H., Jaffrezo, J.-L., Davidson, C. I., Dibb, J. E., Pandis, S. N., Hillamo, R., Maenhaut, W., Kuhns, H. D., and Makela, T.: The contribution of snow, fog and dry deposition to the summer flux of anions and cations at Summit, Greenland, J. Geophys. Res., 100, 16275–16288, 1995.

Braconnot, P., Otto-Bliesner, B., Harrison, S., Joussaume, S., Peterchmitt, J.-Y., Abe-Ouchi, A., Crucifix, M., Driesschaert, E., Fichefet, Th., Hewitt, C. D., Kageyama, M., Kitoh, A., Laîné, A., Loutre, M.-F., Marti, O., Merkel, U., Ramstein, G., Valdes, P., Weber, S. L., Yu, Y., and Zhao, Y.: Results of PMIP2 coupled simulations of the Mid-Holocene and Last Glacial Maximum – Part 1: experiments and large-scale features, Clim. Past, 3, 261–277, doi:10.5194/cp-3-261-2007, 2007.

Chae, J.-S., Byun, J.-I., Yim, S. A., Choi, H.-Y., and Yun, J.-Y.: ^{7}Be in ground level air in Daejeon, Korea, Radiat. Prot. Dosim., 146, 334–337, 2011.

Conen, F. and Robertson, L. B.: Latitudinal distribution of radon-222 flux from continents, Tellus B, 54, 127–133, 2002.

Dahl-Jensen, D., Johnsen, S. J., Hammer, C. U., Clausen, H. B., and Jouzel, J.: Past accumulation rates derived from observed annual layers in the GRIP ice core from Summit, Central Greenland, in: Ice in the climate system, edited by: Peltier, W. R., NATO ASI Series, Springer, Berlin, Heidelberg, 517–532, 1993.

Dibb, J. D., Meeker, L. D., Finkel, R. C., Southon, J. R., Caffee, M. W., and Barrie, L. A.: Estimation of stratospheric input to the Arctic troposphere: ^{7}Be and ^{10}Be in aerosols at Alert, Canada, J. Geophys. Res., 99, 12855–12864, 1994.

Dibb, J. E.: Vertical mixing above Summit, Greenland: Insights into seasonal and high frequency variability from the radionuclide tracers ^{7}Be and ^{210}Pb, Atmos. Environ., 41, 5020–5030, 2007.

Doering, C.: Measurements of the distribution and behaviour of beryllium-7 in the natural environment, PhD thesis, Queensland University of Technology, Brisbane, Australia, 2007.

Durana, L., Chudy, M., and Masarik, J.: Investigation of Be-7 in the Bratislava atmosphere, J. Radioanal. Nucl. Ch., 207, 345–356, 1996.

Elsässer, C.: Exploration of 10Be ice core records using a climatological model approach: Cosmogenic production versus climate variability, PhD thesis, University of Heidelberg, Heidelberg, Germany, 2013.

Elsässer, C., Wagenbach, D., Weller, R., Auer, M., Wallner, A., and Christl, M.: Continuous 25-years aerosol records at coastal Antarctica – Part 2: Variability of the radionuclides ^{7}Be, ^{10}Be and ^{210}Pb, Tellus B, 63, 920–934, 2011

Feely, H. W., Katzman, D., Seitz, H., Davidson, B., and Friend, J. P.: Final Report on Project StarDust, Report DASA-2166, US Defense Atomic Support Agency, Washington, DC, USA, 1967.

Feely, H. W., Toonkel, L. E., and Larsen, R.: Radionuclides and trace elements in surface air, in: Environmental report, Report EML-395, Environmental Measurements Laboratory, US Department of Energy, 1981.

Feely, H. W., Larsen, R., and Sanderson, C. G.: Annual report of the surface air sampling program, Report EML-440, Environmental Measurements Laboratory, US Department of Energy, 1985.

Feely, H. W., Larsen, R., and Sanderson, C. G.: Annual report of the surface air sampling program, Report EML-497, Environmental Measurements Laboratory, US Department of Energy, 1988.

Fernandoy, F., Meyer, H, Oerter, H., Wilhelms, F., Graf, W., and Schwander, J.: Temporal and spatial variation of stable-isotope ratios and accumulation rates in the hinterland of Neumayer station, East Antarctica, J. Glaciol., 56, 673–687, 2010.

Field, C. V., Schmidt, G. A., Koch, D., and Salyk, C.: Modeling production and climate related impacts on ^{10}Be concentration in ice cores, J. Geophys. Res., 111, D15107, doi:10.1029/2005JD006410, 2006.

Finkel, R. C. and Nishiizumi, K.: Beryllium 10 concentrations in the Greenland Ice Sheet Project 2 ice core from 3–40 ka, J. Geophys. Res., 102, 26699–26706, 1997.

Fischer, H. and Wagenbach, D.: Large-scale spatial trends in recent firn chemistry along an east-west transect through central Greenland, Atmos. Environ., 30, 3227–3238, 1996.

Hamilton, G.: Mass balance and accumulation rate across Siple Dome, West Antarctica, Ann. Glaciol., 35, 102–106, 2002.

HASL: Health and Safety Laboratory environmental quarterly: final tabulation of monthly ^{90}Sr fallout data: 1954–1976, report HASL-329, Energy Research and Development Administration, Health and Safety Laboratory, 1977.

Heikkilä, U. and Smith, A. M.: Production rate and climate influences on the variability of ^{10}Be deposition simulated by ECHAM5-HAM: globally, in Greenland and in Antarctica, J. Geophys. Res., 118, 1–15, 2013.

Heikkilä, U., Beer, J., and Feichter, J.: Modeling cosmogenic radionuclides ^{10}Be and ^{7}Be during the Maunder Minimum using the ECHAM5-HAM General Circulation Model, Atmos. Chem. Phys., 8, 2797–2809, doi:10.5194/acp-8-2797-2008, 2008a.

Heikkilä, U., Beer, J., Jouzel, J., Feichter, J., and Kubik, P.: ^{10}Be measured in a GRIP snow pit and modeled using the ECHAM5-HAM general circulation model, Geophys. Res. Lett., 35, L05817, doi:10.1029/2007GL033067, 2008b.

Heikkilä, U., Beer, J., and Feichter, J.: Meridional transport and deposition of atmospheric ^{10}Be, Atmos. Chem. Phys., 9, 515–527, doi:10.5194/acp-9-515-2009, 2009.

Heikkilä, U., Phipps, S. J., and Smith, A. M.: ^{10}Be in late deglacial climate simulated by ECHAM5-HAM – Part 1: Climatological influences on ^{10}Be deposition, Clim. Past, 9, 2641–2649, doi:10.5194/cp-9-2641-2013, 2013.

Hesshaimer, V.: Tracing the global carbon cycle with bomb radiocarbon, PhD thesis, Institute of Environmental Physics, University of Heidelberg, Germany, 1997.

Horiuchi, K., Uchida, T., Sakamoto, Y., Ohta, A., Matsuzaki, H., Shibata, Y., and Motoyama, H.: Ice core record of ^{10}Be over the past millennium from Dome Fuji, Antarctica: A new proxy record of past solar activity and a powerful tool for stratigraphic dating, Quat. Geochronol., 3, 245–261, 2008.

Ioannidou, A., Manolopoulou, M., and Papastefanou, C.: Temporal changes of ^{7}Be and ^{210}Pb concentrations in surface air at temperate latitudes (40° N), Appl. Radiat. Isotopes, 63, 277–284, 2005.

Johnsen, S. J., Clausen, H. B., Dansgaard, W., Fuhrer, K., Gundestrup, N., Hammer, C. U., Iversen, P., Jouzel, J., Stauffer, B., and Steffensen, J. P.: Irregular glacial interstadials recorded in a new Greenland ice core, Nature, 359, 311–313, 1992.

Johnsen, S. J., Clausen, H. B., Dansgaard, W., Gundestrup, N. S., Hammer, C. U., Andersen, U., Andersen, K. K., Hvidberg, C. S., Dahl-Jensen, D., Steffensen, J. P., Shoji, H., Sveinbjörnsdottir, A. E., White, J. W. C., Jouzel, J., and Fisher, D.: The δ^{18}O record along the Greenland Ice Core Project deep ice core and the problem of possible Eemian climatic instability, J. Geophys. Res., 102, 26397–26410, 1997.

Jouzel, J., Merlivat, L., Pourchet, M., and Lorius, C.: A continuous record of artificial tritium fallout at the South Pole (1954–1978), Earth Planet. Sc. Lett., 45, 188–200, 1979.

Juzdan, Z. R.: Worldwide deposition of ^{90}Sr through 1985, Report EML-515, Environmental Measurements Laboratory, US Department of Energy, 1988.

Koch, D. M. and Mann, M. E.: Spatial and temporal variability of ^{7}Be surface concentrations, Tellus B, 48, 387–396, 1996.

Köhler, P., Muscheler, R., and Fischer, H.: A model-based interpretation of low-frequency changes in the carbon cycle during the last 120 000 years and its implications for the reconstruction of atmospheric Δ^{14}C, Geochem. Geophy. Geosy., 7, Q11N06, doi:10.1029/2005GC001228, 2006.

Kolb, W.: Aktivitätskonzentrationen von Radionukliden in der bodennahen Luft Norddeutschlands und Nordnorwegens im Zeitraum von 1963 bis 1990, report PTB-Ra-29, Physikalisch Technische Bundesanstalt, Braunschweig, Germany, 1992.

Kovaltsov, G. A. and Usoskin, I. G.: A new 3D numerical model of cosmogenic nuclide ^{10}Be production in the atmosphere, Earth Planet. Sc. Lett., 291, 182–188, 2010.

Kubik, P. W. and Christl, M.: ^{10}Be and ^{26}Al measurements at the Zurich 6 MV Tandem AMS facility, Nucl. Instrum. Meth. B, 268, 880–883, 2010.

Kulan, A.: Atmospheric production and transport of cosmogenic ^{7}Be and ^{10}Be, PhD thesis, University of Uppsala, Sweden, 2007.

Kulan, A., Aldahan, A., Possnert, G., and Vintersved, I.: Distribution of ^{7}Be in surface air of Europe, Atmos. Environ., 40, 3855–3868, 2006.

Laj, C., Kissel, C., and Beer, J.: High resolution global paleointensity stack since 75kyr (GLOPIS-75) calibrated to absolute values, in: Timescales of the Paleomagnetic Field, edited by: Channell, J. E. T., Kent, D. V., Lowrie, W., and Meert, J. G., Geophysical Monograph, Vol. 145, American Geophysical Union, Washington DC, USA, doi:10.1029/145GM19, 2004.

Larsen, R. J.: Worldwide deposition of ^{90}Sr through 1983, Report EML-444, Environmental Measurements Laboratory, US Department of Energy, 1985.

Larsen, R. J. and Sanderson, C. G.: Annual report of the surface air sampling program, Report EML-524, Environmental Measurements Laboratory, US Department of Energy, 1990.

Larsen, R. J. and Sanderson, C. G.: EML surface air sampling program, 1989 data, Report EML-541, Environmental Measurements Laboratory, US Department of Energy, 1991.

Larsen, J. L., Sanderson, C. G. and Kada, J.: EML Surface Air Sampling Program 1990–1993 data, Report EML-572, Environmental Measurements Laboratory, US Department of Energy, 1995.

Leifer, R.: Project Airstream: Trace Gas Final Report, Report EML-549, Environmental Measurements Laboratory, US Department of Energy, 1992.

Leifer, R. and Juzdan, R.: The High Altitude Sampling Program: Radioactivity in the Stratosphere – final report, Report EML-458, Environmental Measurements Laboratory, US Department of Energy, 1986.

Leppänen, A.-P., Usoskin, I. G., Kovaltsov, G. A., and Paatero, J.: Cosmogenic ^{7}Be and ^{22}Na in Finland: Production, observed periodicities and the connection to climatic phenomena, J. Atmos. Sol.-Terr. Phy., 74, 164–180, 2012.

Levin, I., Naegler, T., Heinz, R., Osusko, D., Cuevas, E., Engel, A., Ilmberger, J., Langenfelds, R. L., Neininger, B., Rohden, C. v.,

Steele, L. P., Weller, R., Worthy, D. E., and Zimov, S. A.: The global SF6 source inferred from long-term high precision atmospheric measurements and its comparison with emission inventories, Atmos. Chem. Phys., 10, 2655–2662, doi:10.5194/acp-10-2655-2010, 2010a.

Levin, I., Naegler, T., Kromer, B., Diehl, M., Francey, R. J., Gomez-Pelaez, A. J., Schäfer, A., Steele, L. P., Wagenbach, D., Weller, R., and Worthy, D. E.: Observations and modelling of the global distribution and long-term trend of atmospheric $^{14}CO_2$, Tellus B, 62, 26–46, 2010b.

Masarik, J. and Beer, J.: Simulation of particles fluxes and cosmogenic nuclide production in the Earth's atmosphere, J. Geophys. Res., D104, 12099–13012, 1999.

Masarik, J. and Beer, J.: An updated simulation of particle fluxes and cosmogenic nuclide production in the Earth's atmosphere, J. Geophys. Res., 114, D11103, doi:10.1029/2008JD010557, 2009.

Mazaud, A., Laj, C., and Bender, M.: A geomagnetic chronology for antarcticic ice accumulation, Geophys. Res. Lett., 21, 337–340, 1994.

Megumi, K., Matsunami, T., Ito, Kiiyoda, S., Mizohata, A., and Asano, T.: Factors, especially sunspot number, causing variations in surface air concentrations and depositions of ^{7}Be in Osaka, Japan, Geophys. Res. Lett., 27, 361–364, 2000.

Merchel, S., Bremser, W., Akhmadaliev, S., Arnold, M., Aumaître, G., Bourlès, D. L., Braucher, R., Caffee, M., Christl, M., Fifield, L. K., Finkel, R. C. , Freeman, S. P. H. T., Ruiz-Gómez, A., Kubik, P. W., Martschini, M., Rood, D. H., Tims, S. G., Wallner, A., Wilcken, K. M., and Xuh, S.: Quality assurance in accelerator mass spectrometry: Results from an international round-robin exercise for ^{10}Be, Nucl. Instrum. Meth. B, 289, 68–73, 2012.

Muscheler, R., Beer, J., Wagner, G., Laj, C., Kissel, C., Raisbeck, G. M., Yiou, F., and Kubik, P. W.: Changes in the carbon cycle during the last deglaciation as indicated by the comparison of ^{10}Be and ^{14}C records, Earth Planet. Sc. Lett., 219, 325–340, 2004.

Muscheler, R., Beer, J., Kubik, P. W., and Synal, H. A.: Geomagnetic field intensity during the last 60000 years based on ^{10}Be and ^{36}Cl from the Summit ice cores and ^{14}C, Quaternary Sci. Rev., 24, 1849–1860, 2005.

Muscheler, R., Snowball, I., Joos, F., Müller, S., Beer, J., and Vonmoos, M.: Solar activity during the last 1000 yr inferred from radionuclide records, Quanternary Sci. Rev., 27, 82–97, 2007.

Naegler, T.: Simulating bomb radiocarbon: Consequences for the global carbon cycle, PhD thesis, Institute of Environmental Physics, University of Heidelberg, Germany, 2005.

Naegler, T. and Levin, I.: Closing the global radiocarbon budget 1945–2005, J. Geophys. Res., 111, D12311, doi:10.1029/2005JD006758, 2006.

Nishiizumi, K. and Finkel, R. C.: Cosmogenic radionuclides in the Siple Dome A ice core, available at: http://nsidc.org/data/docs/agdc/nsidc0307nishiizumi/index.html (last access: 23 April 2009), 2007.

Nishiizumi, K., Imamura, M., Caffee, M. W., Southon, J. R., Finkel, R. C., and McAninch, J.: Absolute calibration of ^{10}Be AMS standards, Nucl. Instrum. Meth. B, 258, 403–413, 2007.

Oerter, H., Graf, W., Meyer, H., and Wilhelms, F.: The EPICA ice core from Dronning Maud Land: first results from stable-isotope measurements, Ann. Glaciol., 39, 307–312, 2004.

Pedro, J., van Ommen, T. D., Curran, M. A., Morgan, V., Smith, A. M., and McMrrow, A.: Evidence for climate modulation for the ^{10}Be solar activity proxy, J. Geophys. Res., 111, D21105, doi:10.1029/2005JD006764, 2006.

Pedro, J. B., Smith, A. M., Simon, K. J., van Ommen, T. D., and Curran, M. A. J.: High-resolution records of the beryllium-10 solar activity proxy in ice from Law Dome, East Antarctica: measurement, reproducibility and principal trends, Clim. Past, 7, 707–721, doi:10.5194/cp-7-707-2011, 2011.

Pedro, J., McConnell, J. R., van Ommen, T. D., Fink, D., Curran, M. A. J., Smith, A. M., Simon, K. J., Moy, A. D. and Das, S. B.: Solar and climate influences on ice core ^{10}Be records from Antarctica and Greenland during the neutron monitor era, Earth Planet. Sc. Lett., 355, 174–186, 2012.

Pourchet, M., Magand, O., Frezotti, M., Ekaykin, A., and Winther, J.-G.: Radionuclides deposition over Antarctica, J. Environ. Radioactiv., 68, 137–158, 2003.

Raisbeck, G. M., Yiou, F., Fruneau, M., Loiseaux, J. M., Lieuvin, M., Ravel, J. C., and Lorius, C.: Cosmogenic ^{10}Be concentrations in Antarctic ice during the past 30,000 years, Nature, 292, 825–826, 1981.

Raisbeck, G. M., Yiou, F., Jouzel, J., and Petit, J. R.: ^{10}Be and δ^2H in polar ice cores as a probe of the solar variability's influence on climate, Philos. T. Roy. Soc. A, 330, 463–470, 1990.

Roos, P., Holm, R., Persson, R. B. R., Aarkrog, A., and Nielsen, S. P:. Deposition of ^{210}Pb, ^{137}Cs, $^{239+240}$Pu, ^{238}Pu, and ^{241}Am in the Antarctic Peninsula Area, J. Environ. Radioactiv., 24, 235–251, 1994.

Seierstad, I. K., Abbott, P., Bigler, M., Blunier, T., Bourne, A., Brook, E., Buchardt, S. L., Buizert, C., Clausen, H. B., Cook, E., Dahl-Jensen, D., Davies, S., Guillevic, M., Johnsen, S. J., Pedersen, D. S., Popp, T. J., Rasmussen, S. O., Severinghaus, J., Svensson, A., and Vinther, B. M.: Consistently dated records from the Greenland GRIP, GISP2 and NGRIP ice cores for the past 104 ka reveal regional millennial-scale δ18O gradients with possible Heinrich event imprint, Quaternary Sci. Rev. Special Issue: 4th INTIMATE, 106, 29–46, 2014.

Slinn, W. G. N.: Some approximations for the wet and dry removal of particles and gases from the atmosphere, Water Air Soil Poll., 7, 513–543, 1977.

Smith, A. M., Fink, D., Chid, D., Levchenko, V. A., Morgan, V. I., Curran, M., Etheridge, D. M., and Elliott, G.: ^{7}Be and ^{10}Be concentrations in recent firn and ice at Law Dome, Antarctica, Nucl. Instrum. Meth. B, 172, 847–855, 2000.

Sommer, S., Appenzeller, C., Rothlisberger, R., Hutterli, M. A., Stauffer, B., Wagenbach, D., Oerter, H., Wilhelms, F., Miller, H., and Mulvaney, R.: Glacio-chemical study spanning the past 2 kyr on three ice cores from Dronning Maud Land, Antarctica. 1. Annually resolved accumulation rates, J. Geophys. Res., 105, 29411–29421, 2000.

Stanzick, A.: Räumliche und zeitliche Variationen von ^{10}Be und ^{210}Pb in Eisbohrkernen Zentralgrönlands, Diploma thesis, Institute of Environmental Physics, University of Heidelberg, Germany, 1996.

Stanzick, A.: Raum-Zeit-Variationen von Be-10, Pb-210 und Cl-36 in der grönländischen Firndecke: Luft-Firn-Transfer und rezente Trends, PhD thesis, Institute of Environmental Physics, University of Heidelberg, Germany, 2001.

Steig, E. J.: Beryllium-10 in the Taylor Dome ice core: Applications to Antarctic glaciology and paleoclimatology, PhD thesis, University of Washington, USA, 1996.

Steinhilber, F., Abreu, J. A., Beer, J., Brunner, I., Christl, M., Fischer, H., Heikkilä, U., Kubik, P. W., Mann, M., McCracken, K. G., Miller, H., Miyahara, H., Oerter, H., and Wilhelms, F.: 9,400 years of cosmic radiation and solar activity from ice cores and tree rings, P. Natl. Acad. Sci. USA, 109, 5967–5971, 2012.

UNSCEAR: Sources and effects of ionizing radiation, UNSCEAR 2000 Report to the General Assembly, United Nations Scientific Committee on the Effects of Atomic Radiation, available at: http://www.unscear.org/, Vienna, Austria, 2000.

Usoskin, I. G. and Kovaltsov, G. A.: Production of cosmogenic ^{7}Be isotope in the atmosphere: Full 3-D modeling, J. Geophys. Res., 113, D12107, doi:10.1029/2007JD009725, 2008.

Usoskin, I. G., Galina, A., Bazilevskaya, A., and Kovaltsov, G. A.: Solar modulation parameter for cosmic rays since 1936 reconstructed from ground-based neutron monitors and ionization chambers, J. Geophys. Res., 116, A02104, doi:10.1029/2010JA016105, 2011.

Vonmoos, M., Beer, J., and Muscheler, R.: Large variations in Holocene solar activity: Constraints from ^{10}Be in the Greenland Ice Core Project ice core, J. Geophys. Res., 111, A10105, doi:10.1029/2005JA011500, 2006.

Wagner, G., Beer, J., Masarik, J., Muscheler, R., Kubik, P. W., Mende, W., Laj, C., Raisbeck, G. M., and Yiou, F.: Presence of the Solar de Vries Cycle ($\sim$ 205 years) during the Last Ice Age, Geophys. Res. Lett., 28, 303–306, doi:10.1029/2000GL006116, 2001a.

Wagner, G., Laj, C., Beer, J., Kissel, C., Muscheler, R., Masarik, J., and Synal, H. A.: Reconstruction of the paleoaccumulation rate of central Greenland during the last 75kyr using the cosmogenic radionuclides ^{36}Cl and ^{10}Be and geomagnetic field intensity data, Earth Planet. Sc. Lett., 193, 515–521, 2001b.

Wershofen, H. and Arnold, D.: Radionuclides in ground-level air in Braunschweig – report of the PTB Trace Survey Station from 1998 to 2003, PTB-Ra-45, PTB Braunschweig, ISSN 0341-6747, ISBN 3-86509-431-7, 2005.

Yiou, F., Raisbeck, G. M., Bourles, D., Lorius, C., and Barkov, N. I.: ^{10}Be in ice at Vostok Antarctica during the last climatic cycle, Nature, 316, 616–617, doi:10.1038/316616a0, 1985.

Yiou, F., Raisbeck, G. M., Baumgartner, S., Beer, J., Hammer, C., Johnsen, S., Jouzel, J., Kubik, P. W., Lestringuez, J., Stievenard, M., Suter, M., and Yiou, P.: Beryllium 10 in the Greenland Ice Core Project ice core at Summit, Greenland, J. Geophys. Res., 102, 26783–26794, 1997.